LBL-18413
UC-94c c.1

Lawrence Berkeley Laboratory

UNIVERSITY OF CALIFORNIA

RECEIVED
LAWRENCE
BERKELEY LABORATORY
NOV 20 1984
LIBRARY AND
DOCUMENTS SECTION

APPLIED SCIENCE DIVISION

A SEMICONDUCTOR ELECTROCHEMISTRY APPROACH TO THE STUDY OF OXIDE FILMS ON NICKEL ELECTRODES
Final Report

M.J. Madou, S. Wing, and M.C.H. McKubre

September 1984

For Reference
Not to be taken from this room

APPLIED SCIENCE DIVISION

LBL-18413 c.1

Prepared for the U.S. Department of Energy under Contract DE-AC03-76SF00098

DISCLAIMER

This document was prepared as an account of work sponsored by the United States Government. While this document is believed to contain correct information, neither the United States Government nor any agency thereof, nor the Regents of the University of California, nor any of their employees, makes any warranty, express or implied, or assumes any legal responsibility for the accuracy, completeness, or usefulness of any information, apparatus, product, or process disclosed, or represents that its use would not infringe privately owned rights. Reference herein to any specific commercial product, process, or service by its trade name, trademark, manufacturer, or otherwise, does not necessarily constitute or imply its endorsement, recommendation, or favoring by the United States Government or any agency thereof, or the Regents of the University of California. The views and opinions of authors expressed herein do not necessarily state or reflect those of the United States Government or any agency thereof or the Regents of the University of California.

LBL-18413

A SEMICONDUCTOR ELECTROCHEMISTRY APPROACH TO THE STUDY OF OXIDE FILMS ON NICKEL ELECTRODES

Final Report

September 1984

by

M.J. Madou, S. Wing and M.C.H. McKubre

Physical Electronic Department
Engineering Sciences Laboratory
Stanford Research Institute
Menlo Park, California 94025

for

Technology Base Research Project
Lawrence Berkeley Laboratory
University of California
Berkeley, California 94720

This work was supported by the Assistant Secretary for Conservation and Renewable Energy, Office of Energy Systems Research, Energy Storage Division of the U.S. Department of Energy under Contract No. DE-AC03-76SF00098, subcontract no. 4514810 with the Lawrence Berkeley Laboratory.

ABSTRACT

Impedance measurements and photoeffect studies on nickel electrodes were carried out to characterize the oxide films on such electrodes. These measurements revealed some interesting fundamental aspects of NiO electrode behavior. We found that, depending on the electrode potential, an n-type or p-type semiconducting oxide can be present at the surface of a nickel electrode, giving rise, respectively, to anodic or cathodic photocurrents under illumination. Impedance measurements show that a solid-state diffusion process, presumably of protons through the oxide film, dominates the impedance behavior for the charged electrode; for the discharged electrode, the impedance behavior is dominated by the space charge inside the p-type oxide. We demonstrated that by using semiconductor electrochemistry techniques new fundamental insights about the kinetics of battery electrodes can be obtained (for example, a diagram for the interfacial energetics of a Ni/NiO electrode was derived from the above measurements).

The emphasis in this project more recently has been the elucidation of the role of additives to both electrode and electrolyte on the charge/discharge kinetics. Semiconductor electrochemistry type techniques (such as photocurrent measurements, Mott-Schottky measurements, etc.), as well as cyclic voltammetry, have been used extensively to that end. All the additives tested are impurities of importance that influence battery performance; some for the better, most for the worse.

All additives to the alkaline electrolyte were tested on three types of electrodes: bare nickel, NiO single crystal, and NiO (thick film). We also incorporated the impurities in the thick film (an electrodeposited NiO film) by adding the same additives to the electrodeposition solution. By using these different electrode types, we were able to determine the effects of various additives and to distinguish surface effects, catalytic stoichiometric, or bulk electrode effects. If, for example, the influence of additives in the case of $Ni(OH)_2$ is a surface effect, then it can be enhanced by the use of film electrodes, which are very thin as contrasted to normal structures in which bulk properties are more pronounced.

Although our results should be tested on actual production quality battery plates, it appears that manufacturing could benefit from some of our findings. For example, we found $CoSO_4$ additives to the alkaline electrolyte to be better for increasing electrode capacity than codeposition of cobalt onto the nickel electrode.

This report is submitted as the final technical report on Subcontract 4520910 under Contract DE-AC03-76SF00098.

CONTENTS

LIST OF ILLUSTRATIONS..... vii

LIST OF TABLES..... ix

ABSTRACT..... iii

FOREWORD..... x

INTRODUCTION TO THE KINETICS OF THE NICKEL ELECTRODE IN KOH WITH AND WITHOUT LiOH..... 1

APPARATUS AND METHODS (CELL, ELECTRODE, ELECTROLYTES, AND ELECTRODE SURFACE PRETREATMENT)..... 3

Cell and Electrodes..... 3

Electrolyte Preparation..... 5

Electronic Equipment..... 5

Electrode Surface Preparation..... 8

PREPARING THICK NiO FILMS..... 9

Growth of NiO in 35 Wt% KOH..... 9

Growth of NiO in NaOCl..... 11

Electrodeposition of NiO..... 11

Growth of NiO in Glycol..... 12

Growth of NiO on a Vitreous Carbon Electrode..... 13

Conclusion..... 13

CYCLIC VOLTAMMOGRAMS IN THE DARK..... 15

Untreated Nickel Electrodes..... 15

The Passivation Region..... 15
The Charge/Discharge Region..... 18
Restructuring Effect..... 19

Treated Nickel Electrodes..... 20

The Passivation Region..... 20
The Charge/Discharge Region..... 20
The Charge/Discharge Region for a Heat-Treated Electrode..... 21
Single Crystal NiO Electrodes..... 23

PHOTOEFFECTS ON NICKEL ELECTRODES..... 27

IMPEDANCE MEASUREMENTS ON NICKEL ELECTRODES..... 33

EFFECT OF LITHIUM ADDITION..... 43

EFFECT OF ADDITIVES ON THE NICKEL ELECTRODE..... 45

Introduction..... 45

Lithium..... 46

Iron..... 50

Cobalt..... 54

Zinc..... 58

Barium..... 58

Nickel..... 58

REFERENCES..... 67

ILLUSTRATIONS

1 Cyclic Voltammograms, 100 mV s^{-1}, 35 wt% KOH, Surface Area = 0.452 cm^2 ω = 12.22 Hz..... 4

2 AC Impedance Measurement System..... 6,7

3 Total Charging Charge (Q_a) as a Function of Final Anodic Growing Voltage (V_a)..... 10

4 Cyclic Voltammogram of Untreated Nickel Electrode, 50 mV s^{-1}, KOH 23.3 wt%, LiOH 4.8 wt%, ω = 12.22 Hz, Surface Area = 0.452 cm^2..... 16

5 Cyclic Voltammogram, 20 mV s^{-1}, KOH 23.3 wt%, LiOH 4.8 wt%, ω = 10 Hz, (Surface Area = 0.452 cm^2) Showing Peaks in Passivation Region..... 17

6 Cyclic Voltammogram of Several Cycles, 50 mV s^{-1}, KOH 23.3 wt%, LiOH 4.8 wt%, ω = 10 Hz, Surface Area = 0.452 cm^2..... 17

7 Cyclic Voltammograms Showing Increasing Anodic Excursion Limit, 20 mV s^{-1}, KOH 23.3 wt%--LiOH 4.8 wt%, ω = 10 Hz (Surface Area = 0.452 cm^2)..... 18

8 Cyclic Voltammograms of Increasing Film Thickness; 20 mV s^{-1}, KOH 23.3 wt%--LiOH 4.8 wt%, ω = 10 Hz (Surface Area = 0.452 cm^2)..... 21

9 Cyclic Voltammograms Showing Restructuring Effect, 20 mV s^{-1}, KOH 23.3 wt%--LiOH 4.8 wt%, ω = 10 Hz Surface Area = 0.452 cm^2, C-Type Film..... 22

10 Cyclic Voltammogram, 20 mV s^{-1}, KOH 23.3 wt%--LiOH 4.8 wt%, ω = 10 Hz, Surface Area = 0.452 cm^2 on a C-Type Film After Heating the Sample for 16 Hours at 130°C..... 23

11 Cyclic Voltammograms on Single-Crystal NiO (100) Plane, 100 mV s^{-1}..... 25

12 Photocurrent (ΔI) as a Function of Time at Constant Chopper Speed..... 28

13 Photocurrent (ΔI) as a Function of Time at Different Chopper Speeds but Constant Potential (-1.350 V vs SHE)..... 29

14 Photocurrent (ΔI) as a Function of Time at Constant Potential (+1.25 V vs SHE)..... 31

15 Nyquist Plot for Applied Potenial of -0.32 V vs SHE..... 34

16 Expanded Nyquist Plot for Applied Potential of -0.32 V vs SHE..... 36

17 Nyquist Plot for Applied Potential of +0.61 V vs SHE..... 36

18 Bode Plot for Applied Potential of -0.785 V vs SHE..... 36

19 Bode Plot for Applied Potential of +0.614 V vs SHE..... 37

20 Plot of X^2 vs V vs SHE for a Ni Electrode in 35 wt% KOH..... 38

21 Energy Diagram for Ni(II) Oxide at pH = 14 Together with Fermi-Levels for Cathodic Decomposition ($E_{c,cdc}$), H^+/H_2 and O_2/H_2O..... 42

22 Tests of Additives to $Ni(OH)_2$ Reported in the Literature..... 45

23 Effect Over Time of Lithium Additive on Cyclic Voltammograms for C-Type NiO Film, 50 mV s^{-1}..... 47

24 Effect of Lithium Additive on Cyclic Voltammograms, 50 mV s^{-1}..... 48

25 Effect of Iron Additive on Cyclic Voltammograms, 50 mV s^{-1}..... 51

26 Effect of Cobalt Additive on Cyclic Voltammograms, 50 mV s^{-1}..... 55

27 Effect of Zinc Additive on Cyclic Voltammograms, 50 mV s^{-1}..... 59

28 Effect of Barium Additive on Cyclic Voltammograms, 50 mV s^{-1}..... 63

TABLES

1 Preparation of NiO Electrodes..... 12

2 Charge Capacities for Different NiO Electrodes in 35 Wt% KOH..... 13

3 Test of Additives to Various Types of NiO Electrodes..... 46

FOREWORD

Although considerable applied and fundamental work has been reported on iron, nickel, zinc, and to a lesser extent on cadmium, controversy still exists about the charge storage mechanisms for these systems. One of the more outstanding problems concerns the precise nature of charge storage on nickel. Nickel electrodes require additives to obtain the combination of properties attributed to them: high efficiency, chemical stability, and a long life cycle. Yet, the exact role of the additives is not understood. Similar unresolved problems exist for the other three battery electrodes. Understanding the mechanisms of the effect of additives, as well as the kinetics of the battery reactions, could benefit battery manufacturers by revealing better and cheaper additives for increasing battery performance and by suggesting different modes of plate preparation [and battery configurations in general]. However, actual battery electrode plates have a porous structure, so the ratio of electrolyte volume/electrode surface area will be much smaller than that employed in the experiments reported here. In this work we have attempted to investigate charge storage mechanisms using a combination of classical electrochemistry and semiconductor electrochemistry techniques. In the first year of the program, which is covered by this report, we have concentrated on the nickel electrode.

The report is divided into two major parts: the first seven sections address the kinetics of the nickel electrode in alkaline solutions (KOH with or without LiOH added); The section entitled "Effect of Additives on the Nickel Electrode" deals with the effect of additives to the alkaline electrolyte.

INTRODUCTION TO THE KINETICS OF THE NICKEL ELECTRODE
IN KOH WITH AND WITHOUT LiOH

For several decades, work on the nickel electrode has been oriented to its battery applications. Recent publications have focused attention on more fundamental problems. It is generally accepted that cycling of a nickel electrode in alkaline solutions involves the following phases:

$$\begin{array}{ccc} \alpha\text{-Ni(OH)}_2 & \rightleftharpoons & \gamma\text{-NiOOH} \\ \downarrow & & \uparrow \\ \beta\text{-Ni(OH)}_2 & \rightleftharpoons & \beta\text{-NiOOH} \end{array}$$

The α-$Ni(OH)_2$ is unstable on standing on open circuit or cycling and is converted irreversibly to β-$Ni(OH)_2$. Charging the electrode converts the divalent β-phase to an oxidation state larger than +3 (γ-NiOOH or β-NiOOH). The β-phase NiOOH can be more completely discharged and is thus capable of higher charging efficiency and utilization. (The greater involvement of K^+ ions in the phase hinders complete reduction to $Ni(OH)_2$ in the case of γ-NiOOH.) Diffusion of reacting ions, primarily protons, plays an essential part in the mechanism. McArthur (1) found $D_{H+} = 3.1 \times 10^{-10}$ and 4.6×10^{-11} cm^2/s for H^+ passing through the reduced and oxidized material.

Of particular importance in battery operation is the oxygen evolution in the charge and overcharge conditions. At standard conditions

$$Ni(OH)_2 + OH- = NiOOH + H_2O + e- \quad ,$$

has a potential (relative to Hg/HgO) of $E^o = 0.41$ V, as compared with the oxygen evolution

$$4OH- = O_2 + 2H_2O + 4e- \text{ at } E^o = 0.307 \quad .$$

Fortunately for battery operation, the latter reaction has a higher overvoltage, which may be influenced by the presence of impurities or additives.

It is well recognized that the electrochemical processes at the nickel electrode are greatly influenced by the presence of surface oxides. Both the charged and discharged state of the nickel electrode are oxides of nickel, and a number of studies have been performed to determine the influence of lithium ions on the solid-state properties of

these passivating oxide films. The ac response of nickel oxides has been studied in detail by, for example, Glarum and Marshall (2) and Zimmerman et al (3). Ellipsometric measurements of oxide films in nickel were performed by Hopper and Ord (4). MacArthur, as mentioned above, determined a proton diffusion coefficient for the NiOH electrode (1). Cyclic voltammetry on the nickel electrodes has been carried out extensively by, for example, Arvia et al (5-7).

The different theories put forward to explain the positive influence of LiOH on capacity, potential, and life of the NiO electrode rely on solid-state properties of the passivating films. In this context, Tichenor (8) pointed out that the lithium influence could be explained as a doping effect of lithium in NiO, under the assumption that the oxide involved is a p-type semiconductor. Tuomi (9), on the other hand, pointed out that the effect cannot be explained on the basis of the p-type character of one of the oxides, because the important oxide in the charged region (β-NiOOH) is an n-type semiconductor. Weiniger (10) explains the effect of Li^+ differently; by penetrating into the crystal lattice, Li^+ ions prevent K^+ ions from doing so. The effect is an increase in oxygen overvoltage because the recombination of adsorbed oxygen is hindered, allowing greater charge acceptance. (Further on, we will discuss more possible explanations for this beneficial Li^+ effect.)

Chernykh and Yakovleva (11) found both anodic and cathodic photocurrents at oxidized nickel electrodes. These photocurrents were attributed to n- and p-type nickel oxides, respectively. Angelini et al. (12) show anodic and cathodic photopotentials for nickel and discuss a fast and a slow component of the observed photopotential. They assume that the faster photopotential component is due to the separation of electron-hole pairs within the electric field in the oxide and that the slow process is due to decomposition of surface oxides.

In view of the important influence of the solid-state properties of the oxide films in the nickel electrode behavior, we decided to approach the study using methods that reveal more about the bulk and surface properties of the nickel oxides. The experimental methods used in the present study were primarily photocurrent measurements as a function of voltage, wavelength, and chopper speed, and ac impedance measurements as a function of frequency and voltage. Measurements were performed on surface-formed passivating oxides and on electrodeposited films. We expected that semiconductor effects would be more readily observable with thicker films.

APPARATUS AND METHODS (CELL, ELECTRODE, ELECTROLYTES, AND ELECTRODE SURFACE PRETREATMENT)

Cell and Electrodes

An all-Teflon® cell was used for performing impedance measurements, coulometry, and cyclic voltammetry. The reference electrode [in most cases a Zn/Zn(II) couple] was placed in an external reservoir to prevent contamination of the working electrolyte. As a counterelectrode we used a platinum wire, also placed in a separate compartment. Provision was made in the working electrode chamber to purge with high purity N_2 to eliminate dissolved O_2 and exclude CO_2. For the light experiments an all-quartz cell was used with all three electrodes in the same compartment. The light source was a mercury vapor pressure lamp (PEK Model 912-0, power supply M702). Potentials were usually recalculated and expressed with respect to the standard hydrogen electrode (SHE).

Electrodeposited nickel oxide films of different thickness on nickel were prepared according to a procedure described by Briggs et al (13). The room-temperature electrodeposition of the oxide by this method is effected by anodic/cathodic cycling of the metal substrate in an aqueous solution containing 0.1N $NiSO_4$, 0.1N NaAC, and 0.001N KOH ("Briggs solution"). A different thickness of deposit can be obtained by varying the cycling procedure. The films used in our experiments were usually those described by Briggs as Procedure C and Procedure F films. To determine qualitatively the relative thickness of the oxide films on nickel, we used coulometry; the amount of charge under the large anodic peak in cyclic voltammograms, such as shown in Figure 1, was measured. It is accepted in the literature (14) that this peak corresponds to the oxidation of $Ni(OH)_2$ to β-NiOOH (charging peak). For the bare nickel surface cycled in a 35 weight percent (wt%) KOH solution, at a sweep rate of 100 mV s^{-1}, 11 mC cm^{-2} would be typically associated with this peak [see Figure 1(b)]; the value would be 62 mC cm^{-2} for a C-type film [see Figure 1(a)] and 176 mC cm^{-2} for an F-type film (not shown). The smaller anodic peak in Figure 1 has been associated with oxidation of nickel to $Ni(OH)_2$, and the single cathodic (discharge) peak has been attributed to the reduction of a β-NiOOH back to $Ni(OH)_2$.

For the dark measurements, temperatures were stabilized by immersing the working and auxiliary vessels in a thermostatically controlled water/ethylene-glycol bath.

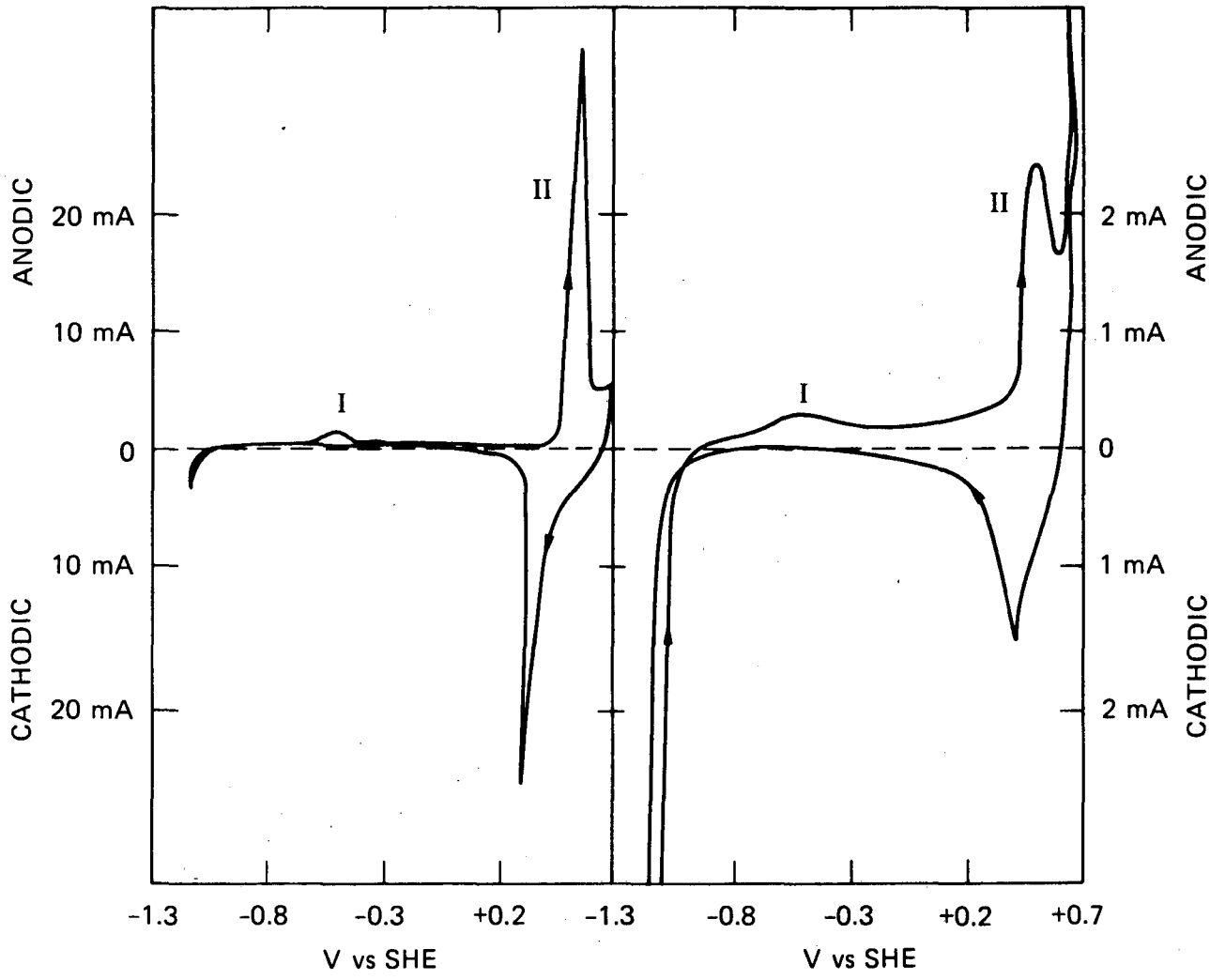

(a) Treated sample (C-type film, observe y-axis)

(b) Untreated sample

JA-350522-176

FIGURE 1 CYCLIC VOLTAMMOGRAMS, 100 mV s^{-1}, 35 wt% KOH, SURFACE AREA = 0.452 cm^2
ω = 12.22 Hz

Electrolyte Preparation

Electrolytes were prepared in polyethylene containers with analytical grade chemicals and doubly distilled deionized water. For the impedance work, and for coulometry and cyclic voltammetry in the Teflon cell, special care was taken to exclude CO_2 and O_2. This precaution was not taken for the light experiments, which were performed in an open quartz cell, but fresh solutions were made up regularly.

Electronic Equipment

Measurements of the electrochemical transfer function (15,16) (the "ac impedance") of the nickel oxide/electrolyte system were performed using a Solartron Model 1172/1183/1185 frequency response analyzer (FRA). Figure 2(a) shows schematically the experimental configuration employed for impedance measurements. The FRA is controlled by an Apple II microcomputer via an IEEE-488 bus (17). This setup permits us to perform measurements over a range of frequencies (10^{-4} to 10^{4} Hz) and dc voltages in a single experiment, thus facilitating the determination of Mott-Schottky plots (18). The software written to control the FRA and for subsequent data reduction and deconvolution is presented in (19).

A Princeton Applied Research Model 175/173 potentiostat was used for both potentiodynamic cycling and ac impedance studies. In order to offset inherent limitations of the potentiostat and FRA, a novel interface between these units was designed and built. The circuit diagram is shown as Figure 2(b), and the function is described in detail in (19). The important features of this unit briefly are as follows:

- Provides automatic "back-off" of the dc component of the voltage applied between the working and reference electrodes, thus allowing greater precision in the measurement of the ac signal.
- Measures the current as the voltage drop across an R-C parallel standard, in series with the counterelectrode. This minimizes the double limitations of poor high frequency response of the PAR current-to-voltage converter (17), and the difficulty of handling large voltages that occur at high frequencies under potentiostatic conditions when the current is transduced by a resistor or simple current clamp.
- Attenuates the FRA ac output, allowing measurement to be made with < 10 mV excitation.
- Provides the high input impedance and low input capacitance necessary for the determination of semiconductor impedances.

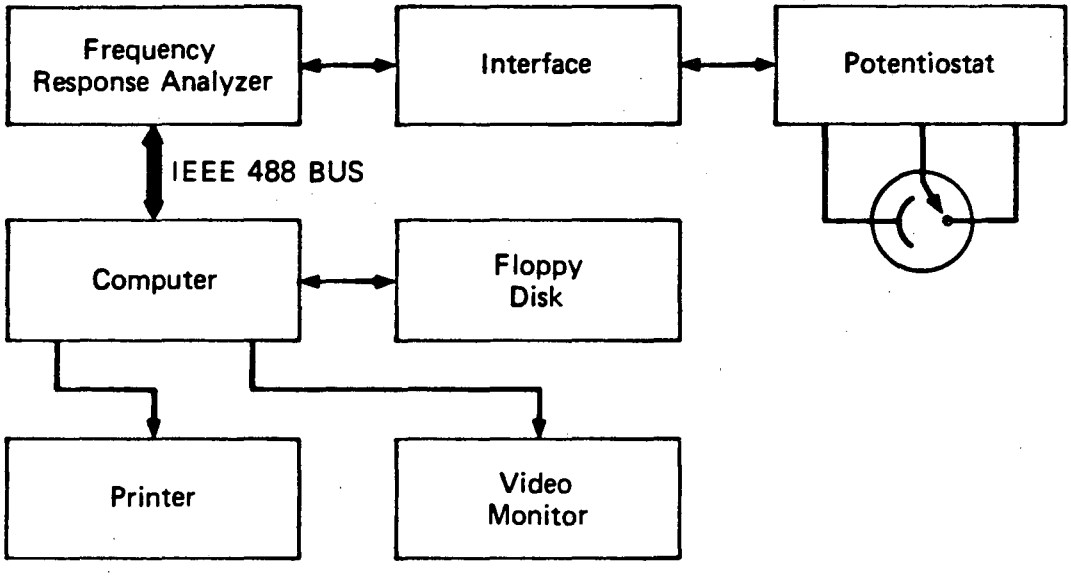

(a) SCHEMATIC DIAGRAM OF INSTRUMENTATION

JA-350583-51A

FIGURE 2 AC IMPEDANCE MEASUREMENT SYSTEM

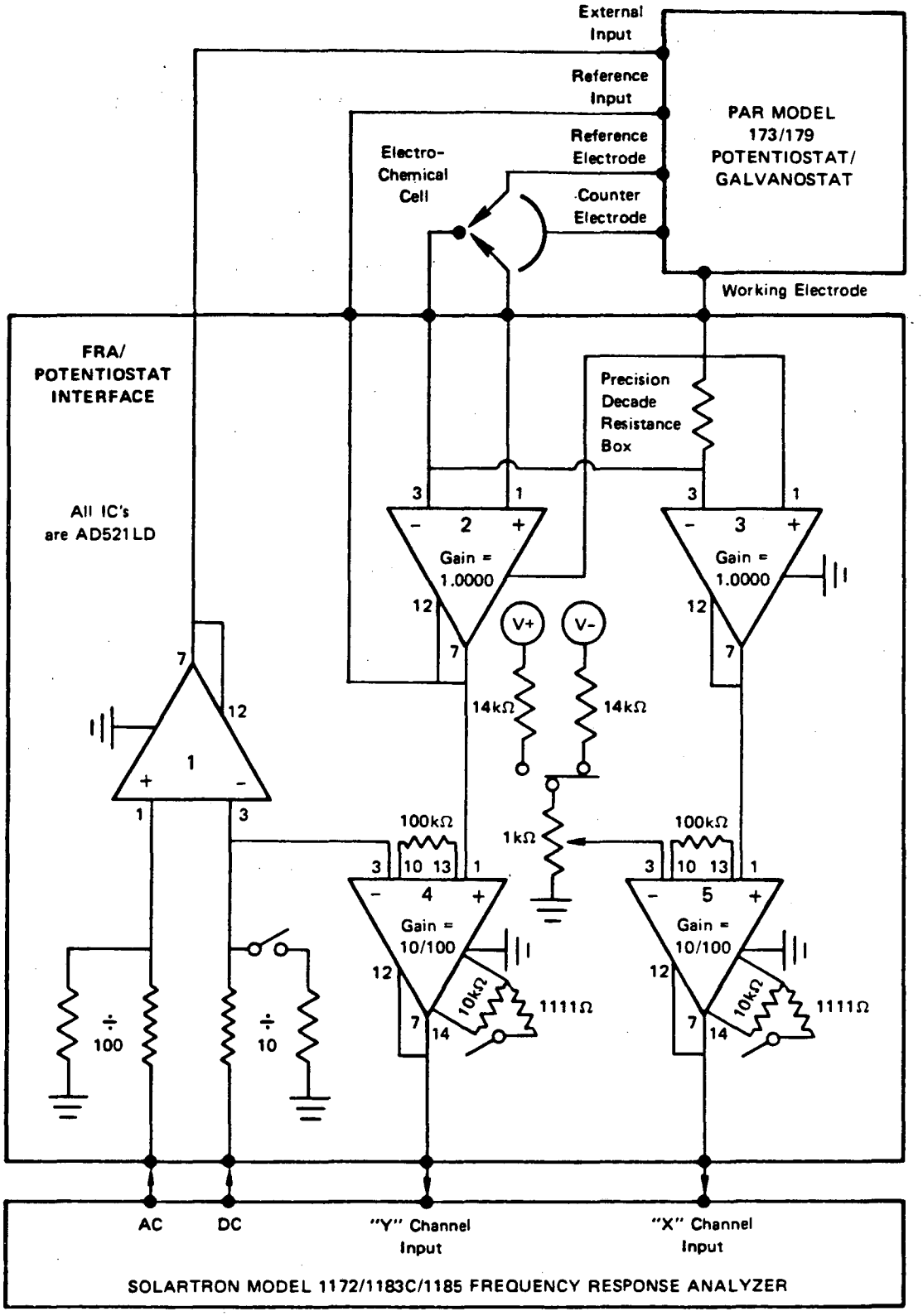

(b) FRA/POTENTIOSTAT INTERFACE UNIT CIRCUITRY

JA-1535-10

FIGURE 2 IMPEDANCE MEASUREMENT SYSTEM (Concluded)

Electrode Surface Preparation

A nickel electrode manually polished on emery 2/0 paper usually gave an anodic charging ($Ni^{++} \rightarrow$ higher oxidation state) plateau and a cathode discharging (higher oxidation state $\rightarrow Ni^{++}$) peak in a 35 wt% KOH solution. Polishing the nickel electrode manually with an Al_2O_3 (1 μm)/H_2O slurry on a polishing cloth before the experiments resulted in cyclic voltammograms with better-defined peaks. We therefore decided on this latter polishing technique before each experiment.

PREPARING THICK NiO FILMS

The goal was to prepare NiO films in different thicknesses, to distinguish between bulk effects and surface effects and to better isolate the semiconductor properties of the film. Different techniques were attempted: Coulometry was used to estimate the thickness.

Growth of NiO in 35 Wt% KOH

We have tried to determine the effect of applied potential on thickness of the film and to estimate the thickness of the "natural" oxide in concentrated KOH. We thought it might be possible to find a correlation between film thickness and the final anodic growing voltage ($d \sim V_a$).

The electrode potential was slowly (10 mV s^{-1}) brought from -1.171 V vs SHE toward the final growing voltage V_a; the potential was then cycled between +0.679 V vs SHE and +0.129 V vs SHE at 100 mV s^{-1}, after reaching a certain V_a. The total anodic charge (Q_a) and total cathodic charge (Q_c) were determined. Before each new anodic potential scan the electrode was held at -1.171 V vs SHE (in the hydrogen evolution potential range) for 5 minutes. [The total discharging charge (Q_c) accumulates even after several minutes at +0.679.] Because the reasons for the sluggish reduction process are not well understood, we usually preferred Q_a as an indicator of the thickness.

Figure 3 gives an example of the dependence of total anodic charge (Q_a) on final anodic growing voltage (V_a). After the experiments described above, a film could be seen on the nickel electrode surface. It is clear from Figure 3 that, at least over a limited voltage range, Q_a is strongly dependent on V_a. [note that the region where such a dependence is desired is the region where our impedance measurements indicate the existence of a field inside the oxide (see below)].

Recently, Glarum et al. (2) made films in 1M KOH with charge capacities of 50 mC/cm^2, which is more than double our maximum charge capacity for films formed potentiostatically in concentrated alkali. In their case, the nickel electrode was pulsed between -1.4 and +0.65 V vs SHE. One second was spent at each potential per pulse. Several minutes sufficed to produce films with 50 mC/cm^2 charge capacity.

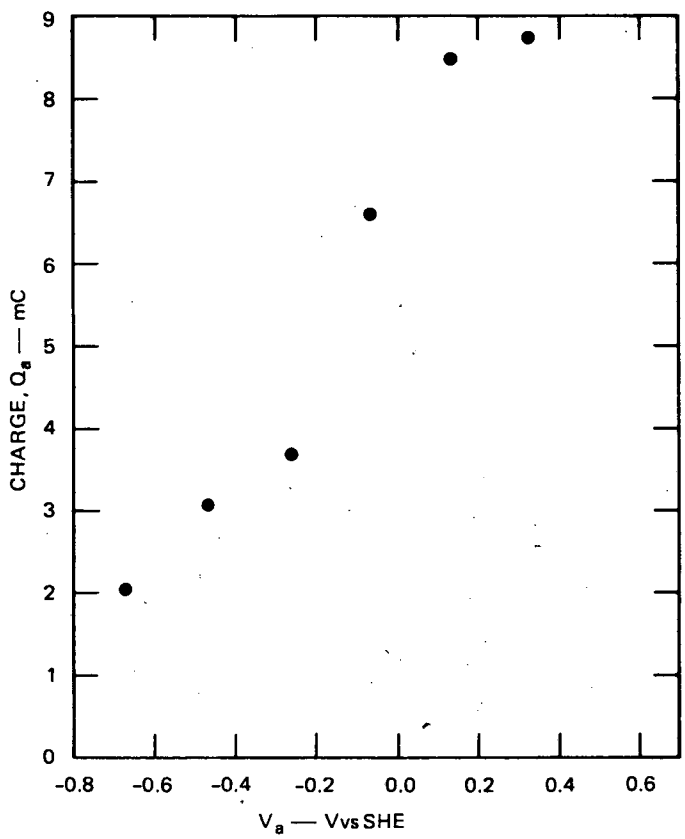

FIGURE 3 TOTAL CHARGING CHARGE (Q_a) AS A FUNCTION OF FINAL ANODIC GROWING VOLTAGE (V_a)

Solution 35 wt% KOH, surface area 0.452 cm^2

Other methods we used enabled us to obtain films with charge capacities greater than 100 mC/cm^2, so we did not spend more time by trying to form films as described by Glarum et al (2). The importance of their experiments is that films of NiO can be grown in concentrated alkali solutions without the addition of soluble nickel species.

To grow an oxide by anodically/cathodically cycling in a pure KOH solution, the applied current must be sufficient to drive the potential of the nickel electrode far enough into hydrogen and oxygen evolution. Indeed, when applied currents are not higher than 100 $\mu A\ cm^{-2}$, as in experiments by Hopper et al. (4), there is no increase in charge capacity and presumably no increase in thickness. We believe that this points to a dissolution/precipitation mechanism for oxide growth by cycling. We have shown (at 45°C at least) on a rotating ring disc detector (RRDE) that, at large anodic disc potentials (into the oxygen evolution region), a soluble nickel species can be detected at the ring

(20). D.M. MacArthur (21) has observed soluble nickel species in highly alkaline solutions at 45°C on the rotating ring disc, he speculates that the soluble specie is an oxyhydroxide, which, in some very active form, dissolves into the electrolyte. This specie, he says, must be distinguishable from the oxyhydroxide produced during the normal oxidation of NiOH, since the latter is not soluble. We suggest that this soluble nickel specie is electroreduced or precipitated onto the nickel electrode surface and left there in an "active" state, so that it is more easily oxidized. Hopper et al. (4) believe that the oxide actually grows by cycling even at low currents, but their argument is based upon optical measurements. At their low current levels, the potential excursions are not far enough into hydrogen and oxygen evolution, and (especially) the anodic voltage does not go positive enough to allow formation of any soluble nickel species, thus making oxide growth impossible. This explains why a thicker oxide can be formed with cycling in an alkaline solution than by our method described in Figure 3; our polarization is never anodic enough to allow the formation of some soluble nickel species.

For a freshly polished nickel electrode, the smallest Q_c observed was still approximatly 1 mC cm^{-2}. To measure Q_c in this case, the electrode was first held at -1.171 V vs SHE, then stepped to +0.129 V vs SHE and cycled between +0.129 V vs SHE and +0.679 V vs SHE at 100 mV s^{-1}. When this was done repeatedly without polishing the electrode between cycles, Q_c increased gradually, indicating further growth of NiO--either chemically at -1.171 V vs SHE or during cycling between +0.129 V vs SHE and +0.679 V vs SHE. Both processes make the interpretation and usage of Figure 3 as the thickness indicator more difficult.

Growth of NiO in NaOCl

There are several other methods of preparing thick NiO films; one is chemical attack of nickel in NaOCl. The nickel surface is first cleaned with glass paper. The NaOCl in our case was reagent grade, containing 10 percent available chlorine, and the temperature was between 70°C and 80°C. We found that the reaction did not start easily, and that when it started, there was copious formation of loose, black nickel oxide, never really leaving a good film behind on the nickel surface. Moreover, after the process, several deep etch pits were observed on the nickel surface. We did not try further to use this method.

Electrodeposition of NiO

Although it is clear from discussions above that films of NiO can be grown in alkaline solution, thicker layers may be produced if nickel salts are added to the solution (13). If we assume a dissolution/precipitation model for oxide formation we can see the addition of nickel salts as a means of precipitating more active nickel on the nickel electrode, which subsequently oxidizes rapidly, yielding a thicker film than when all the "active" nickel stems from dissolution of

the electrode. We conducted experiments with a Briggs solution consisting of 0.1N $NiSO_4$, 0.1N NaAc, and 0.001N KOH in water. The room-temperature electrodeposition of the oxide was effected by anodically/cathodically cycling the metal substrate in the above solution. Depending on the cycling procedure a different thickness of deposit was obtained; the thinner films were uniform and adherent. The films used in our experiments were generally those described by Briggs as procedure C and procedure F films (see Table 1).

Table 1

PREPARATION OF NiO ELECTRODES

Film Type	Charge Density (mA/cm^2)	Cycle	Duration of Anodic and Cathodic Treatments	Nickel Content ($atom/cm^2 \times 10^6$)
C	0.5	1-4	1	1.0-1.3
	0.5	5-7	2	
	0.5	8-10	4	
F	2	1-4	1/2	3.4-3.8
	2	5-7	1	
	2	3-10	2	
	2	11	4	

Source: (13)

Figure 1 showed the dramatic change in the cyclic voltrammogram in Figure 1 taken in 35 wt% KOH before and after treatment in the Briggs solution. The film used for this example was a procedure C film. Figure 1(a) is the cyclic voltammogram for the treated sample. Figure 1(b) is the cyclic voltammogram for the untreated sample. The total charge (Q_a) was much bigger in the case of the treated sample [Figure 1(a)]. This clearly reflects the gain in deposited material for such an electrode.

The cyclic voltammograms shown here are those obtained after several cycles. Indeed, especially between the first and following cycles the peaks in the charge/discharge region shift and change drastically (such "restructuring" effects are discussed later in this report). Table 2 shows a comparison of Q_a in 35 wt% KOH for a bare nickel electrode, and for a procedure C and procedure F film after several cycles. Because the procedure F film usually peeled in strong KOH, we generally used procedure C films when working in 35 wt% KOH.

Table 2

CHARGE CAPACITIES FOR DIFFERENT NiO ELECTRODES
IN 35 Wt% KOH

Electrode Type	α_A (mC/cm^2) (100 mV/s sweep rate)	Remarks
Bare nickel	11	Elecrode appears metallic
Procedure C film	62	Turns black after a few cycles in 35 wt% KOH
Procedure F film	176	The black film often peeled in 35 wt% KOH

Growth of NiO in Glycol

We hoped to form thick oxides on nickel in analogy with the procedure for oxidation of silicon in glycol (with a small percentage of water and a stable inorganic salt added), in the same type of solution. Several attempts at different constant current levels failed to give any appreciable oxide growth. In this respect, nickel behaves much like platinum and iridium, in the sense that its oxide cannot sustain a prolonged appreciable ionic current density through the oxide. In the steady state, after reaching a certain oxide thickness, the anodic processes favored are those involving electronic currents by oxidation e.g. H_2. The NiO acquires the conductivity in the charge/discharge region; from then on further oxide growth is difficult, since it is impossible to obtain the high field strengths necessary to drive the ions.

Growth of NiO on a Vitreous Carbon Electrode

In order to eliminate possible effects of substrate nickel we also applied our most successful electrodeposition (procedure C) on a polished vitreous carbon electrode. The oxide on vitreous carbon was patchy, but still yielded considerable charge capacity. Typically, the cyclic voltammogram looked like the cyclic voltammograms in Figure 1, but without the small first cathodic peak in the passivation region. This is expected, since the peaks in that potential region are associated with passivation of the bare nickel. Some experiments with electrodeposited $Ni(OH)_2$ on vitreous carbon will be described later in this report.

Conclusion

Electrodeposition of NiO from the Briggs solution was found to be the best method for obtaining reliable and uniformly thick oxide films with charge capacities up to 0.2 C cm^{-2}. During our oxidation studies it became clear that up to a certain field-strength the oxide growth is field-strength dominated, but once the charging region is reached a dissolution/precipitation mechanism takes over.

In further work we would like to deposit NiO films on inert substrates and to perform the same kind of heat treatment and photocurrent studies as reported below for NiO films on nickel.

CYCLIC VOLTAMMOGRAMS IN THE DARK

Untreated Nickel Electrodes

Figure 4 shows a typical example of a cyclic voltammogram on an untreated nickel electrode. We will designate Region I as the passivation region and Region II as the charge/discharge region.

The Passivation Region

There are at least three peaks in Region I. In Figure 5 we designate them as peak a, b, and c. The experiments described in Figure 6 give us some insight in assigning peaks to either H_2 or passivation-related phenomena. When cycling only past peak a, no anodic peak appears; extending the potential scan to include peak b gives rise to peak c. Clearly, peak b and c are related. It seems reasonable to assume that b involves oxidation of nickel and c the reduction of the oxide. Peak a is presumably related to oxidation of hydrogen; when, after cycle 1, the negative excursion is limited to -0.9 V vs SHE, the peak gradually disappears (see cycles 2 to 5). Peak a is more and more pronounced after a long hold time at negative bias, which gives additional support for this hypothesis.

Our claim that the passivating film is at least partially reducible is of considerable consequence in the subsequent discussion. This reduction process apparently has not been previously described. Figure 7 shows why the cathodic peak c goes easily unnoticed. When the anodic excursion limit is progressively increased, peak c becomes a shoulder of the hydrogen reduction onset and finally merges together with that onset. In the same figure, comparison of 7(c) with 7(d) indicates again that peak a is most probably related to hydrogen oxidation. Indeed, with a long cathodic hold, as for Figure 7(d) peak, a appears again (as in Figure 6). Looking back at Figure 4, it is important to notice the crossover at cathodic potentials; after having been anodic, the hydrogen reduction onset is indeed drifted toward more cathodic potentials. This shows that hydrogen evolution on the passivated nickel electrode has a larger overvoltage than on the cathodically held nickel electrode. The cathodic charge involved in the reduction of $Ni(OH)_2$ was difficult to determine because of the accompanying hydrogen evolution at most voltages. The possibility of growing oxides with repetitive cycling between anodic and cathodic, as mentioned above in this report, indicates that not all of the $Ni(OH)_2$ is reduced.

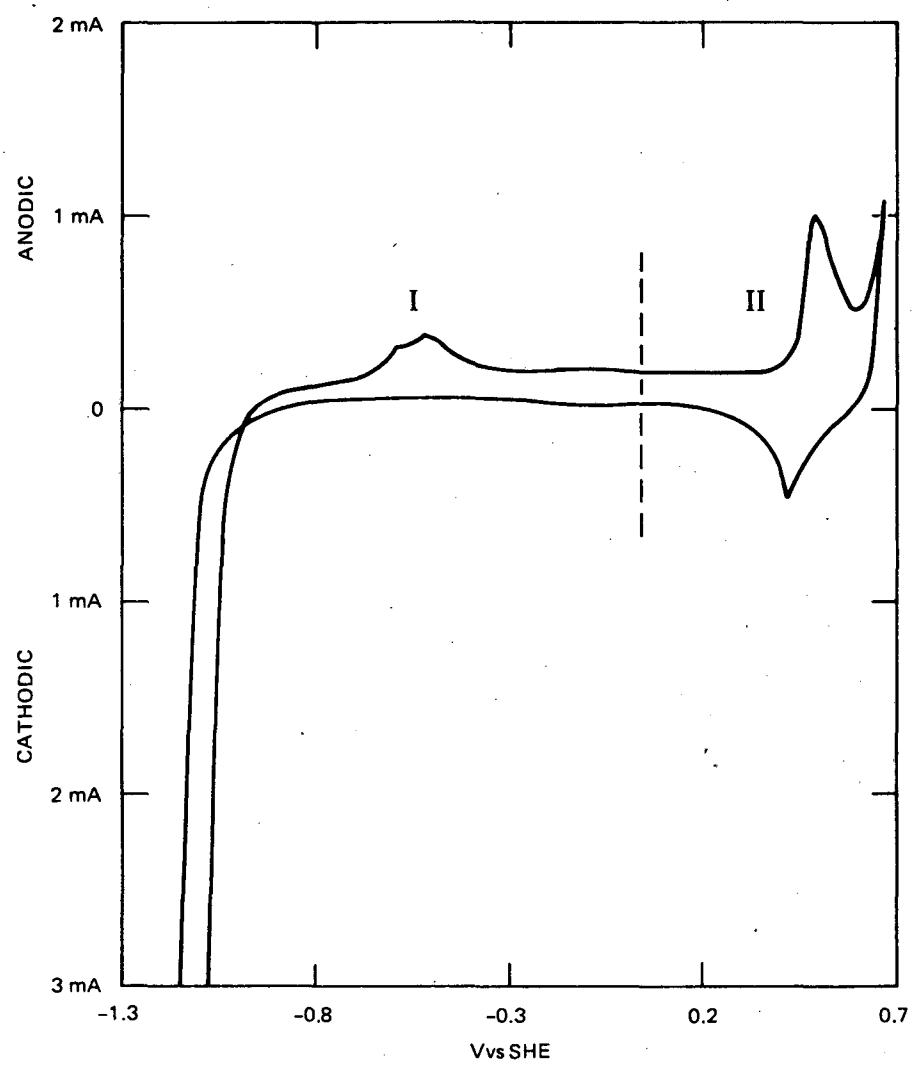

FIGURE 4 CYCLIC VOLTAMMOGRAM OF UNTREATED NICKEL ELECTRODE, 50 mV s^{-1}, KOH 23.3 wt%, LiOH 4.8 wt%, $\omega = 12.22$ Hz, SURFACE AREA = 0.452 cm^2

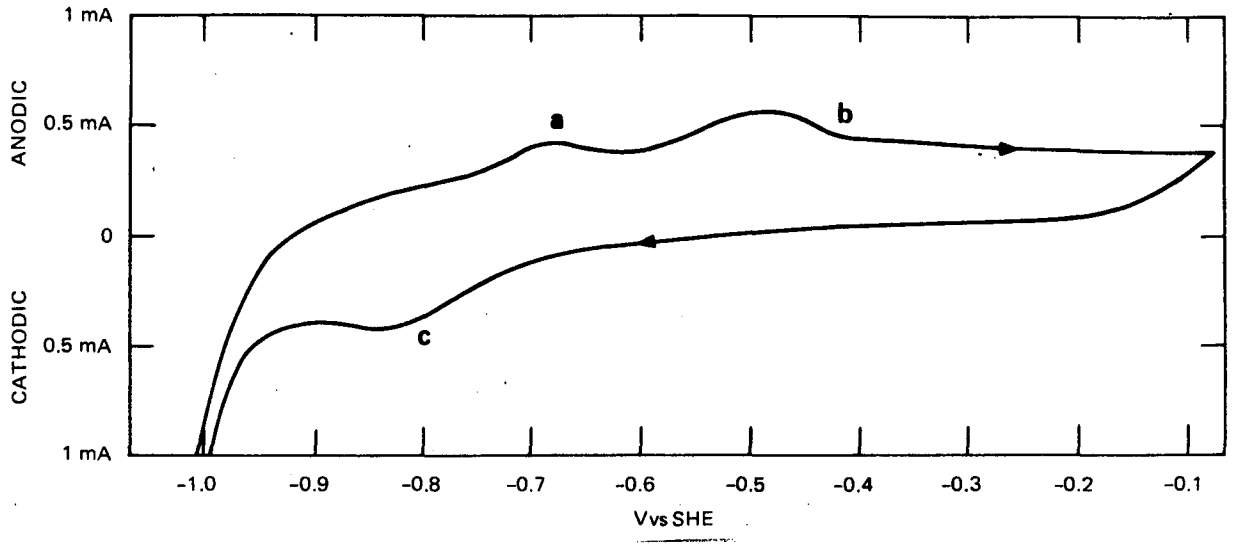

FIGURE 5 CYCLIC VOLTAMMOGRAM, 20 mV s^{-1}, KOH 23.3 wt%, LiOH 4.8 wt%, $\omega = 10$ Hz, (SURFACE AREA = 0.452 cm^2) SHOWING PEAKS IN PASSIVATION REGION

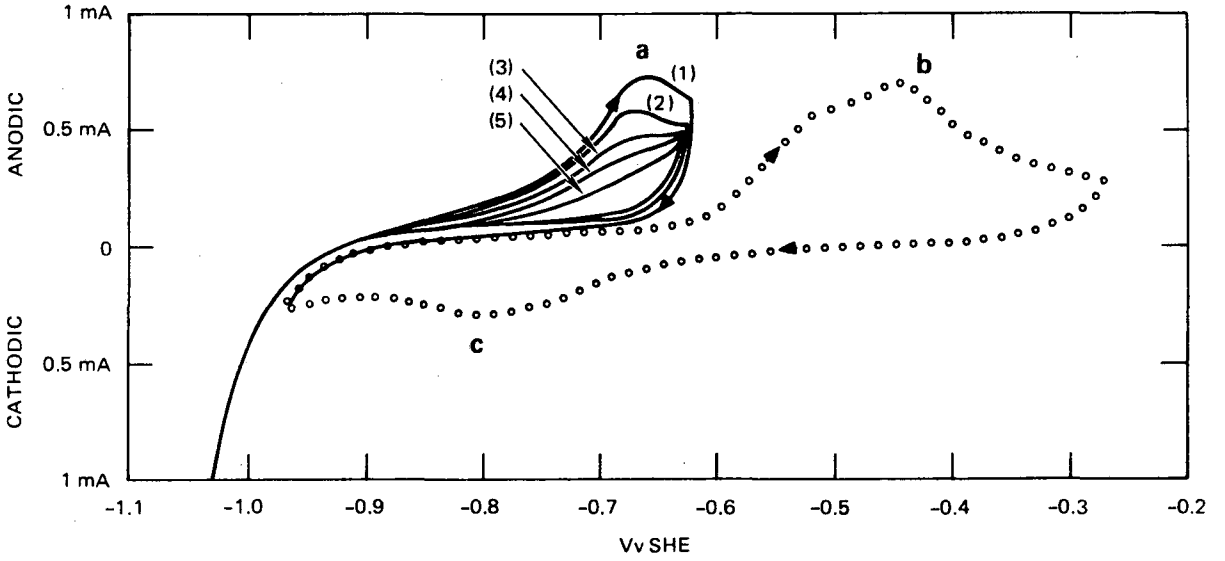

FIGURE 6 CYCLIC VOLTAMMOGRAM OF SEVERAL CYCLES, 50 mV s^{-1}, KOH 23.3 wt%, LiOH 4.8 wt%, ω = 10 Hz, SURFACE AREA = 0.452 cm^2

For cycle (1) the electrode was held at -1.101 Vvs SHE for 5 minutes; for cycle (2) to (5), a continuous sweep was used, starting at -0.9 Vvs SHE.

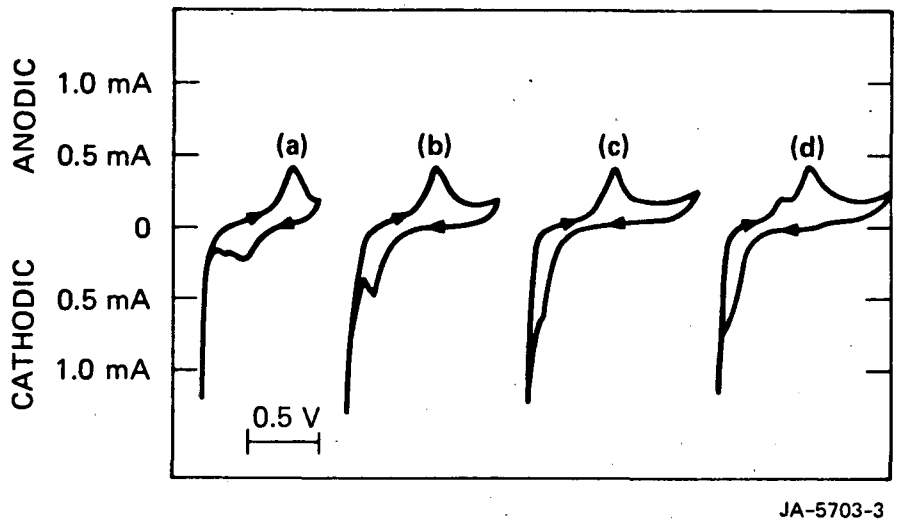

FIGURE 7 CYCLIC VOLTAMMOGRAMS SHOWING INCREASING ANODIC EXCURSION LIMIT, 20 mV s^{-1}, KOH 23.3 wt% – LiOH 4.8 wt%, ω = 10 Hz (SURFACE AREA = 0.452 cm^2)

Although the reduction peak (c) in Figure 6 has been observed first here in a solution containing LiOH, it is not yet clear to us if the presence of the LiOH is related to the appearance of that peak. More detailed comparative studies with cyclic voltammetry in pure KOH are necessary for confirmation.

The Charge/Discharge Region

The charging/discharging peak height was little influenced by rotation speed of the electrode. If there was any influence at all, it was to increase the peak height slightly with increasing rotation speed. This clearly indicates that diffusion limitation occurring in this potential region is not associated with mass transport in the solution. We will address this point again when discussing our impedance results.

Peak height is strongly dependent on sweep rate. The model we will use here as a first attempt to describe the nickel electrode reaction involved in charging and discharging is the same used by D.M. MacArthur (22),

- Electron transfer through the nickel hydroxide is believed to occur rapidly in comparison to proton transfer (the redox reaction Ni(II) $\rightleftharpoons$ Ni(III) is regarded as reversible).
- Protons are released adjacent to the nickel ion sites when Ni(II) is oxidized to Ni(III) and a proton vacancy is created when Ni(III) is reduced to Ni(II).

The rate of the reaction is thus believed to be controlled by the rate of proton transfer. With the assumption of semi-infinite diffusion, the current-voltage relationship for a potential sweep can be written as

$$i_p = 2.7 \times 10^5 n^{3/2} A D^{1/2} c^o \nu^{3/2} \quad , \qquad (1)$$

where i_p (A cm^{-2}) is the peak current, A (cm^2) is the area of the electrode, ν is the scan rate in Vs^{-1}, and c^o is the initial concentration, taken as the number of nickel sites per unit volume and expressed as moles/cm^3. [This is simply the density of the nickel hydroxide film divided by the molecular weight. For this calculation, the molecular weight used was that of α-$Ni(OH)_2 \cdot 2/3\ H_2O$, and the density was taken as 2.5 g/cm^3, the value found by x-ray measurements (22). To get a first crude estimate on values for $c^o\ D^{1/2}$ we averaged some values from plots of i_p as a function of $\nu^{1/2}$ in 23.3 wt% KOH and 4.8 wt% LiOH. Disregarding for the moment the reported influence of thickness of the NiO layer on the slope of i_p as a function of $\nu^{1/2}$ (see Ref. 22), we extracted a value of 5.5×10^{-8} mol cm^{-2} $s^{-1/2}$. We will come back to this value for $c^oD^{1/2}$ later when discussing our ac impedance results and compare it to literature values given for this quantity. Finally, it should be stressed that the charge/discharge process is not so reversible; the peak separation between charging and discharging was found to be around 110 mV at a sweep rate of 100 m Vs^{-1}.

We could find no difference in cyclic voltammograms whether LiOH was added to the KOH solution or not.

Restructuring Effect

For a freshly polished electrode, the first potential scan always gives a charging peak shifted quite a bit towards anodic potentials. Only after a certain number of cycles is a steady shape in the cyclic voltammogram reached with the changing peak position more cathodic. A more or less long hold of the electrode at cathodic potentials gave a cyclic voltammogram similar to the original one. This "restructuring" effect has been described in an earlier SRI report to LBL (23) and was also discussed extensively by Schrebler et al (5). There is still considerable speculation as to the underlying mechanism of this "restructuring" effect. We will give a mechanism explaining the restructuring effect later in this report.

It is interesting to mention here that charge/discharge peaks as discussed above do not exhibit the restructuring effects when measured on single crystal NiO(Li) electrodes. The corresponding reactions in that case appear to occur only at the electrode surface, since the total charge under the peaks corresponds to less than a monolayer (approximately) of the charge for the (100) plane, assuming one electron for each Ni^{2+} ion and an idealized (100) surface orientation with no surface roughness. Although in this report we stress some of the similarities between the kind of $Ni(OH)_2$ studied here and single crystal or mosaic NiO, it is clear that this restructuring constitutes a major difference between these different forms of NiO material.

Treated Nickel Electrodes

The Passivation Region

Figure 1 showed the difference in cyclic voltammograms before and after treatment in a Briggs solution. Comparing the relative magnitude of the passivation peak [$I_p(p)$] to the charging peak [$I_p(c)$] in both cases, it becomes clear that $I_p(p)/I_p(c)$ is much smaller for a treated sample. Because the absolute height of the passivation peaks is similar in both cases, plenty of bare nickel surface is exposed to the electrolyte even for a thick c-type film, indicating a very porous film structure. (A C film on vitreous carbon does not give any peak at all in Region I; this is proof that the peak is associated with passivation of bare nickel).

The Charge/Discharge Region

There are several important differences between the charge/discharge region of a treated electrode and that of an untreated electrode:

- The relative magnitude of the anodic current involved in the oxygen reaction is much less in the case of treated samples. [This was clearly illustrated in Figure 1. Observe the scale factor in comparing Figure 1(a) to Figure 1(b)].
- The thicker the film, the broader the charging and discharging peaks. The anodic and cathodic peaks move further apart, indicating a higher degree of irreversibility as illustrated for a C film and an F film in Figure 8. The current scale in Figure 8 is larger for the procedure F film than for the C-type film.
- The "restructuring effect" was seen to give voltage shifts for the anodic peak of up to 50 mV. This is illustrated in Figure 9 for a C-type film. The big shift toward more anodic potentials occurred after a hold for 5 minutes at -1.071 V vs SHE [Figure 9(b)].
- The differences in charge were shown in Table 2.

Far into oxygen evolution the oxide films always peeled, which was usually accompanied by a stream of a white product leaving the surface. The white product seems unstable and reacts with water. Formation of a white, unstable product was also observed when a too-high anodic current was used to form the oxide. The instability of the product and some literature evidence suggests that the product might be NiO_2. This fits our earlier findings with RRDE (23) that at potentials well into oxygen evolution a soluble nickel species can be formed.

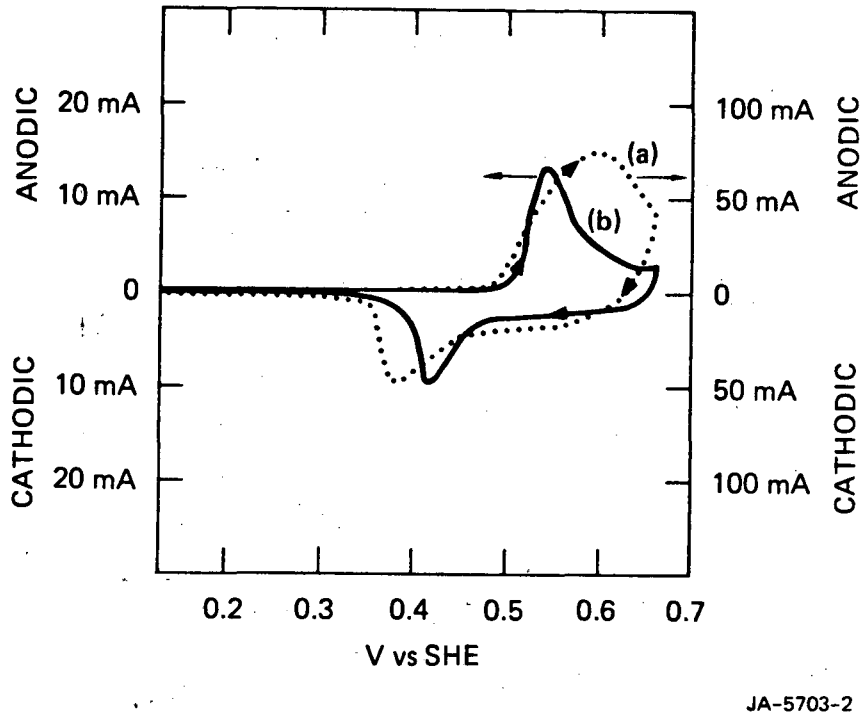

FIGURE 8 CYCLIC VOLTAMMOGRAMS OF INCREASING FILM THICKNESS; 20 mV s^{-1}, KOH 23.3 wt% – LiOH 4.8 wt%, ω = 10 Hz (SURFACE AREA = 0.452 cm^2)

(a: F-type film, b: C-type film)

The Charge/Discharge Region for a Heat-Treated Electrode

In order to understand more about the restructuring effect and the influence of hydration of the passivated layer on electrode behavior, we decided to undertake a series of heat treatment experiments on thick NiO films.

Some very drastic changes occur in the cyclic voltammogram of filmed samples that undergo heat treatment. Our heat treatment consisted simply of heating the samples at 130°C for different lengths of time. In the example shown in Figure 10, a procedure C film was heated for 16 hours at 130°C. Major changes in the cyclic voltammograms can be easily seen by comparing this Figure 10 to Figure 8(b) or to Figure 9(a). In the first cycle, the electrooxidation of the partially dehydrated $Ni(OH)_2$ is appreciably polarized. During cycling (there was a wait of about 1 minute between each cycle), the electrode seems to recover activity and the cyclic voltammograms look more and more like those for a non-heat-treated sample. This result shows the importance of the water content of the colloidal system in the reaction mechanism.

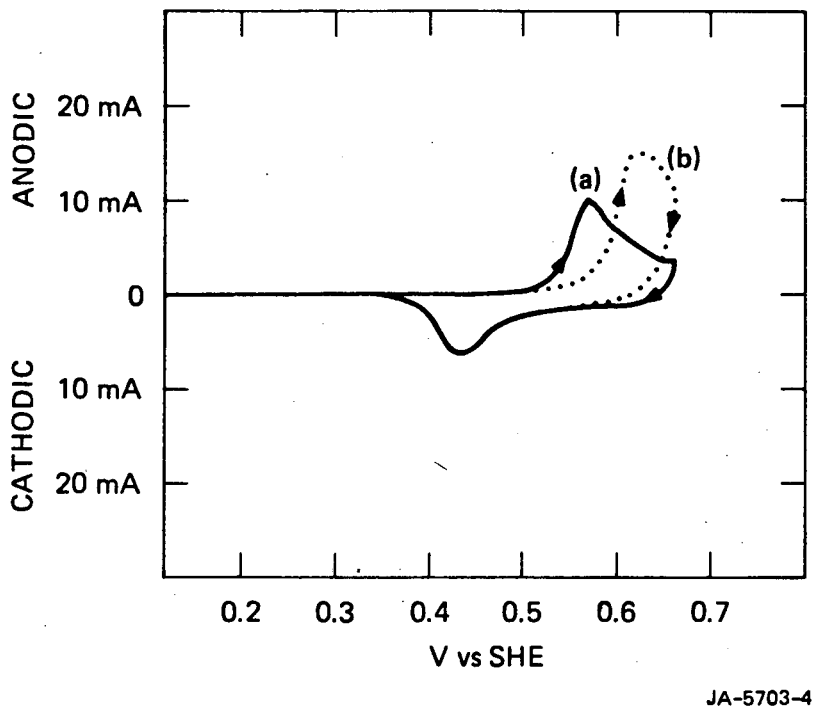

FIGURE 9 CYCLIC VOLTAMMOGRAMS SHOWING RESTRUCTURING EFFECT, 20 mV s^{-1}, KOH 23.3 wt% – LiOH 4.8 wt%, ω = 10 Hz, SURFACE AREA = 0.452 cm^2, C-TYPE FILM

(a: Cyclic voltammogram after several cycles; b: cyclic voltammogram after a hold for 5 minutes at -1.071 Vvs SHE)

Recently Macagno et al. (24) found a very similar behavior for somewhat thinner films of $Ni(OH)_2$ deposited on platinum. The same authors also pointed out that the degree of activation of colloidal $Ni(OH)_2$ is closely related to the amount of water, and that this is consistent with the important role the proton transfer plays in the $Ni(OH)_2$/NiOOH electrochemical reaction.

It is interesting that heat treatment of a $Ni(OH)_2$ film has the same effect as keeping the electrode cathodic or bringing it in solution for the first time (see "restructuring effect"). We believe that the common factor here is a depletion of H_2O or of H^+ inside the oxide film. A freshly formed film dried in N_2 before use or heated at 130°C and a film held cathodic, where protons are consumed in the reduction process, all lead to less H^+ conductivity in the oxide and therefore a larger overpotential for charging of the electrode.

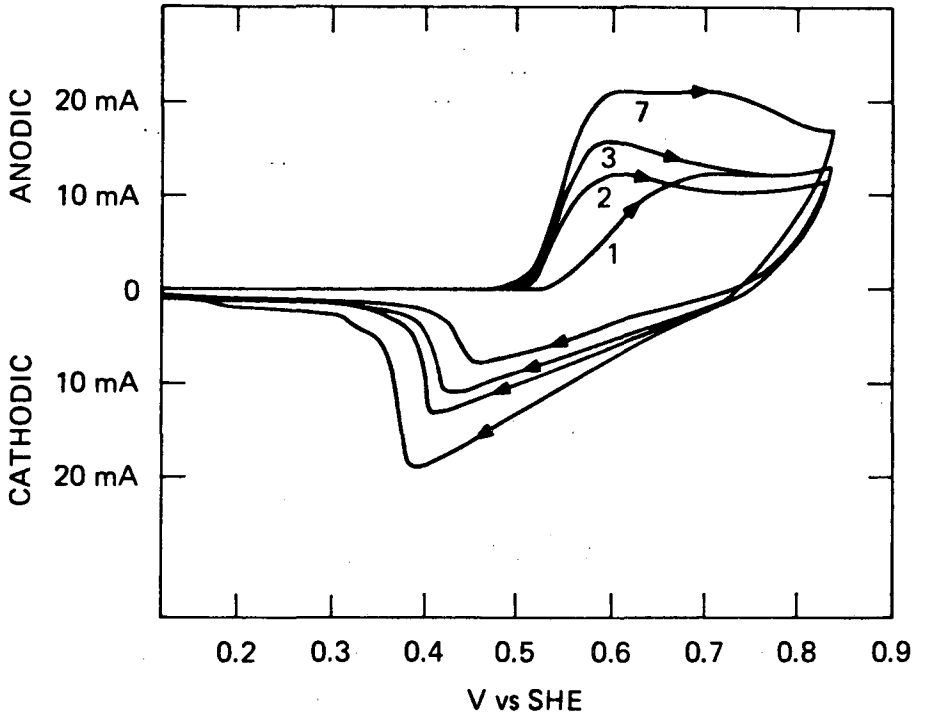

JA-5703-1

FIGURE 10 CYCLIC VOLTAMMOGRAM, 20 mV s^{-1}, KOH 23.3 wt% – LiOH 4.8 wt%, ω = 10 Hz, SURFACE AREA = 0.452 cm^2 ON A C-TYPE FILM AFTER HEATING THE SAMPLE FOR 16 HOURS AT 130°C.

Cycles 1, 2, 3 . . . 7 are consecutive cycles.

For further research it would be interesting to attempt to convert a hydrated $Ni(OH)_2$ by heat treatments to behave like a crystalline NiO electrode. Even after a minor heat treatment, such as described here, currents in the charge/discharge region are lower. Several heat treatments at different temperatures could be tried, after which cyclic voltammograms might show the induced effect.

For the thicker NiO films described here, we could not trace any difference in the charge/discharge in cyclic voltammograms back to the presence of LiOH in solution.

Single Crystal NiO Electrodes

We studied the charge/discharge characteristics on a single crystal NiO electrode (100) plane as a function of pH. No aging or "restructuring" effects were noticed with these types of electrodes, which supports our explanation of the "restructuring effect" having to do with the loss

of water. It is indeed unlikely that a dehydration effect would show up on a monolayer-thick film. These measurements were usually performed with a Hg/HgO reference electrode; since we do not know the correct potential of the electrode vs SHE for the different solutions used here, we did not make our usual conversion to SHE.

Figure 11(a) shows two sets of peaks in acidic medium (1N H_2SO_4). On the basis of their position, we could identify these peaks as corresponding to Ni(II) → Ni(III) and Ni(III) → Ni(IV). D. Yohe et al. (25) came to the same conclusion in another experiment. The charge associated with both peaks corresponds to only a fraction of a monolayer, which is not unexpected since it is doubtful that bulk NiO could be reduced or oxidized. Repeating the cyclic voltammetry experiments in more alkaline solutions caused the two sets of peaks to merge, and at the same time the total charge involved in the process increased substantially [Figure 11(b)] this would indicate that the charge/discharge process on a nickel electrode does involve a mixture of Ni(III) and Ni(IV) oxides. The reason for the increased charge capacity is not well understood, (although the total charge never exceeds a monolayer).

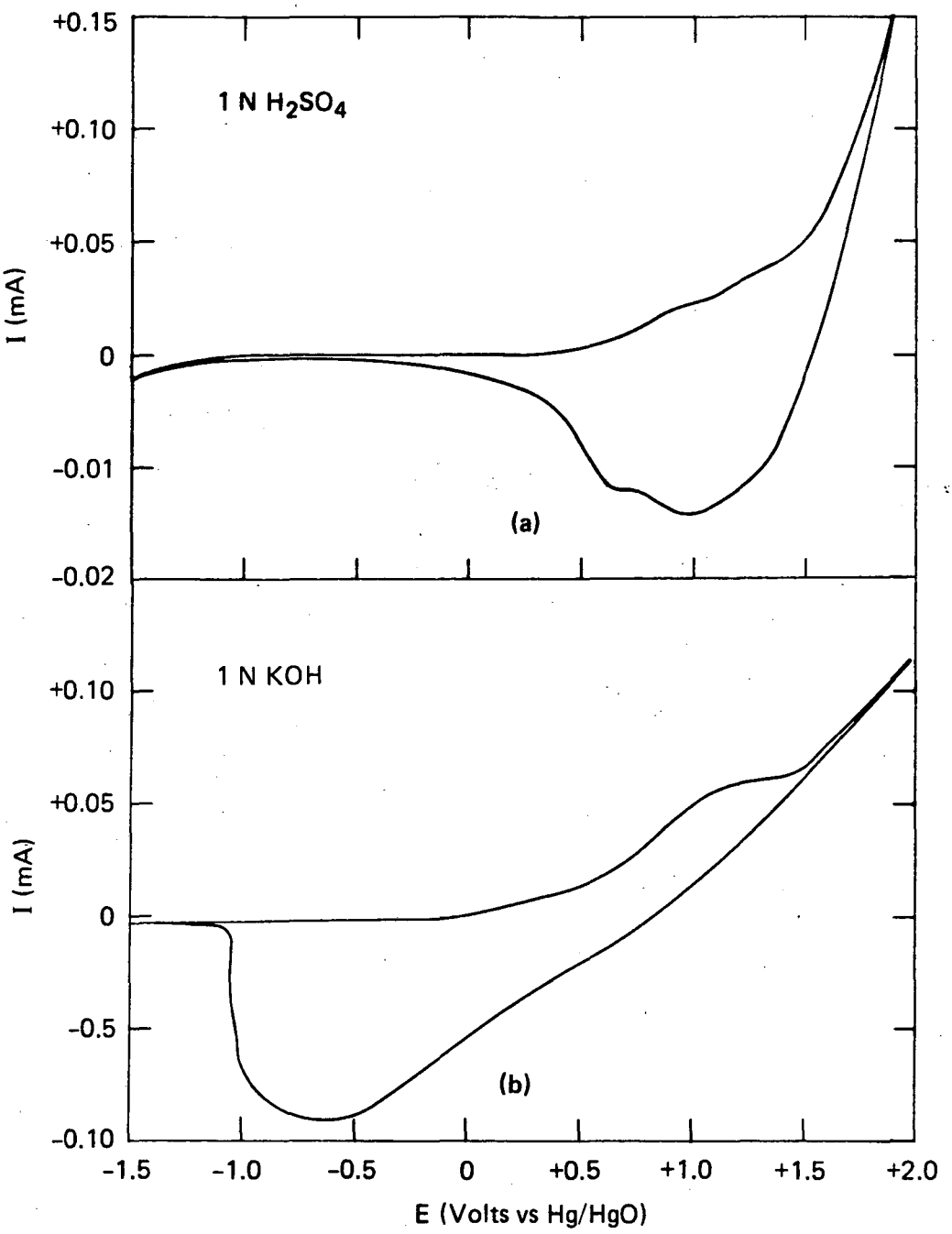

FIGURE 11 CYCLIC VOLTAMMOGRAMS ON SINGLE-CRYSTAL NiO (100) PLANE, 100 mV s^{-1}

PHOTOEFFECTS ON NICKEL ELECTRODES

Crystalline NiO is known to be a p-type semiconductor (26); β-NiOOH is reported to be an n-type semiconductor (9). The sign of the photocurrents found on the nickel electrode under study should indicate the type of the passivating oxides on nickel. Because NiO's bandgap is approximately 3.7 eV (27), light of wavelengths shorter than 3314 Å will be absorbed by a material containing NiO. We could not find a value for the bandgap of β-NiOOH.

We observed both large anodic and large cathodic photocurrents when illuminating a filmed nickel electrode with ultraviolet (UV) light, depending on the applied potential. With the filmed nickel electrode polarized negative with respect to the solution (close to and into the hydrogen evolution range), we found cathodic photocurrents. In this discharge range, the electrode behaved as if it were covered with a p-type semiconducting oxide. With the electrode polarized positive (in the $Ni(OH)_2$ β-NiOOH charge region) large anodic photocurrents were observed, pointing to an n-type passivating oxide layer. We discuss the cathodic photoeffect first.

The measurements represented in Figure 12 were performed on a filmed nickel electrode (F-type film) in the Briggs solution (0.1N $NiSO_4$, 0.1N NaAc, and 0.001N KOH). The light was chopped at a relatively high constant frequency while the potential was progressively made more negative. As shown in Figure 12, the current amplitude increases as the potential becomes more negative. Because the oxide is a p-type oxide, this behavior was not unexpected; indeed, the more negative the applied voltage, the more efficiently electron-hole pairs are separated and the more photocurrent can be expected.

The feature that was less easily understood, in terms of simple p-type semiconductor behavior, is shown in Figure 13, where we present the measured photocurrent as a function of chopper speed for a filmed nickel electrode (C-type film) at a negative potential (-1.35 V vs SHE). A very strong dependence of the photocurrent magnitude on chopper speed is observed, and the lower the chopper speed, the higher the photocurrent. At the highest, and at the lowest, chopper speeds, the photocurrents finally became constant; the amplitude is almost an order of magnitude smaller at the highest chopper speeds. This seems to indicate that two processes affect in the photoresponse of the nickel electrode: a fast-responding photocurrent associated with a semiconducting oxide layer and a much slower, not yet explained process. This is in accordance with the observations by Angelini et al. (12) that there are two

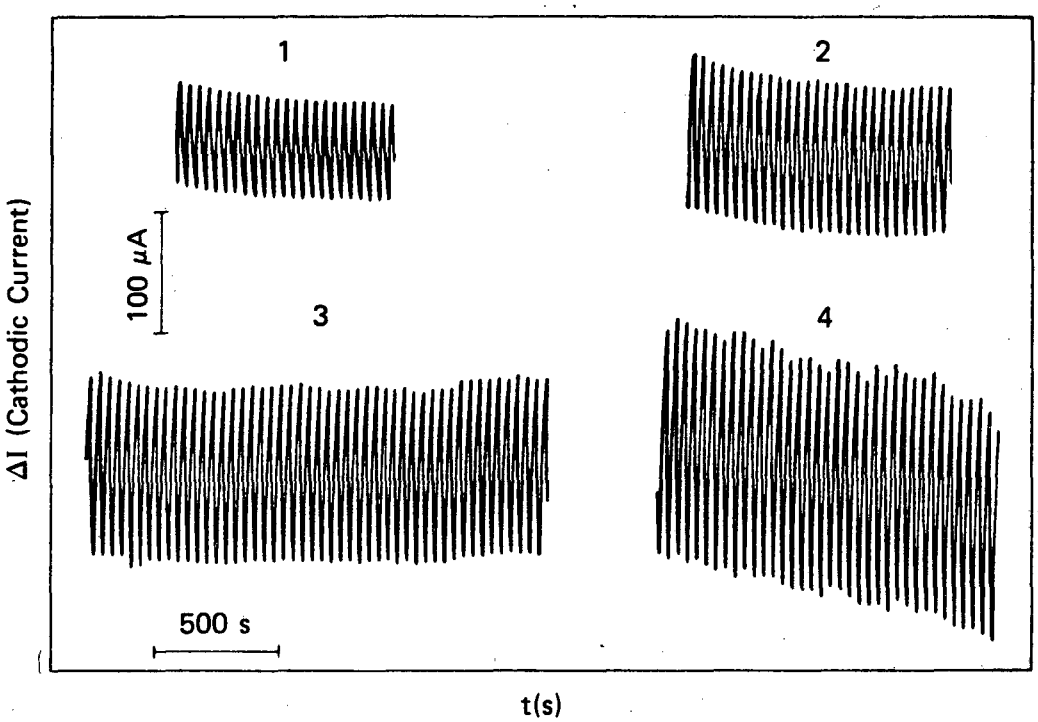

JA-350583-87

FIGURE 12 PHOTOCURRENT (ΔI) AS A FUNCTION OF TIME AT CONSTANT CHOPPER SPEED:

1 -1.112 V vs SHE
2 -1.200 V vs SHE
3 -1.250 V vs SHE
4 -1.350 V vs SHE

Solution: 0.1 N $NiSO_4$, 0.1 N NaAc, 0.001 N KOH (Briggs' solution)
F-type film

components to the photopotential at a nickel electrode. The photocurrent disappears if a filter-absorbing UV (transmission lower than 0.5 percent at wavelengths shorter than 3650 Å) and transmitting visible light is inserted in the light path, which indicates that the photocurrent is UV-induced.

We attempted to measure approximately the absorption edge with a combination of other light filters. With UV-transmitting clear filters (transmission at λ = 3314 Å higher than 85 percent) in place, there was

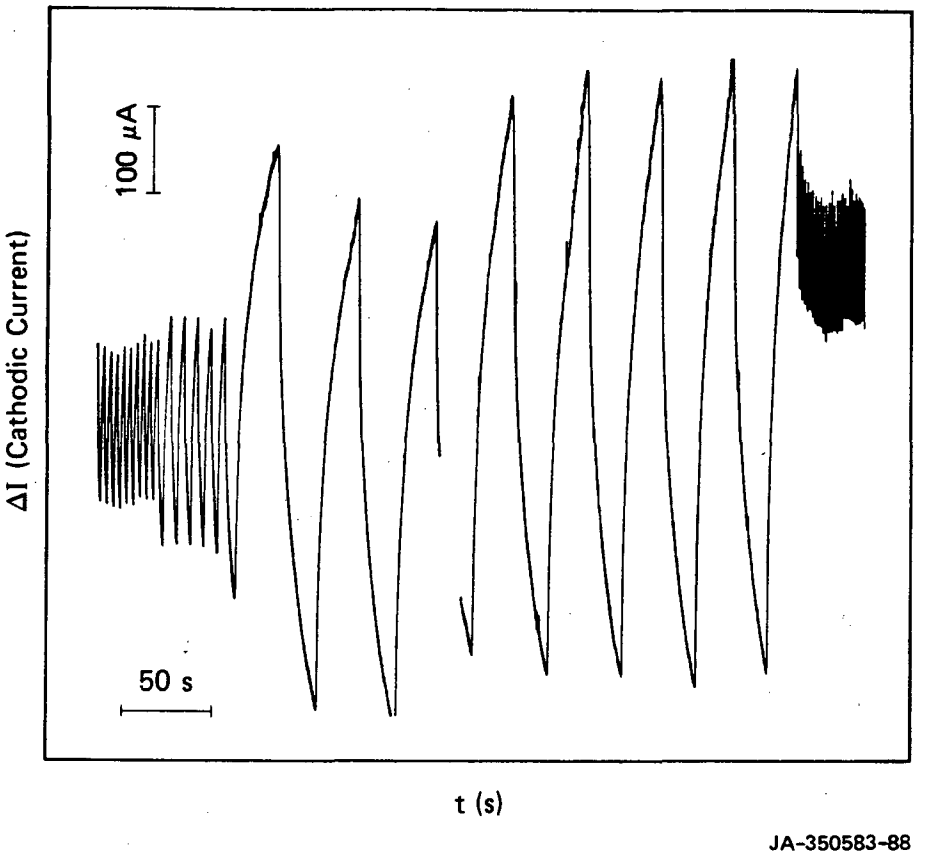

FIGURE 13 PHOTOCURRENT (ΔI) AS A FUNCTION OF TIME AT DIFFERENT CHOPPER SPEEDS BUT CONSTANT POTENTIAL (-1.350 V vs SHE)

Solution: 0.1 N $NiSO_4$, 0.1 N NaAc, 0.001 N KOH (Briggs solution) C-type film

little or no decrease in photocurrent. The data above can accommodate the 3314 Å for the absorption edge of NiO. In the future, a monochromator in combination with a differential technique for measuring the photocurrent will be used to obtain more quantitative data on the absorption edge.

The same photoeffects shown in Figures 12 and 13 were found in 5N KOH and in 35 wt% KOH. More surprisingly, the photoeffect was still present after the film electrode was etched using a 50 wt% HCl solution. In all cases the photocurrents showed the same potential dependence and chopper speed dependence as discussed above for the filmed electrodes. The alkaline solutions used here were chosen because of their practical importance for use in batteries, but obviously the effects described are rather independent of the solutions used.

Our tentative explanation for the two kinds of photoresponses differs from that presented by Angeline et al. (12) and is as follows: Electrons excited by light into the conduction band of a thin layer of oxide reduce mainly protons to hydrogen, but also reduce some Ni(II) oxide to metal at the NiO/electrolyte interface; this corresponds to the fast photoresponse. The overpotential for hydrogen evolution on nickel in the Ni(II) oxide matrix is expected to be lower than on the passivated nickel surface. The longer the light is on, the more nickel forms and the greater the rate of hydrogen evolution; this leads to the slow "photoresponse." When the light is turned off, the nickel slowly passivates again, resulting in an accompanying slow decay of the hydrogen evolution. We suggest that illumination of the nickel electrode gives rise to two distinctively different processes:

(1) A fast-responding primary photoeffect--generation of electron/hole pairs in the semiconducting Ni(II) oxide by UV light, leads, under negative polarization, to increased hydrogen evolution and to some oxide reduction at the oxide/electrolyte interface.

(2) A slow responding pseudophotoeffect--increased current due to hydrogen formation through the reduction of protons on the nickel formed in process (1).

Obviously it is unnecessary to deliberately grow a thick Ni(II) oxide film to see these effects: A native oxide seems sufficient to produce the same effects. The thermodynamic feasibility of the photoreduction of Ni(II) oxide is discussed in the concluding section of this report.

It should be noted that it is generally assumed (14) that Ni(II) oxide cannot be reduced by nickel. We have indirect proof there that such a reduction can occur with optically excited conduction band electrons. As we have seen experimentally, Ni(II) can be reduced to some extent even in the dark.

As stated above, at sufficiently large anodic potentials (in the charging region), a large anodic photocurrent can be observed. This photocurrent for an nickel electrode with an F-type film is shown in Figure 14. Clearly the oxide behaves as an n-type semiconductor in this potential range. As in the case of the cathodic photocurrents, a slow and a fast photoresponse here are observed also. The measurements shown in Figure 14 were performed in the Briggs solution; the same kind of photoresponse was observed in 5N KOH or with unfilmed surfaces. Using the light effect as a probe to determine the nature of the mixed oxide in the charging region as a function of voltage might be very useful in understanding the more fundamentally important electrode reactions involved in the charge/discharge of the nickel electrode. The photocurrents seen here might be attributed to n-type β-NiOOH described by Tuomi (9).

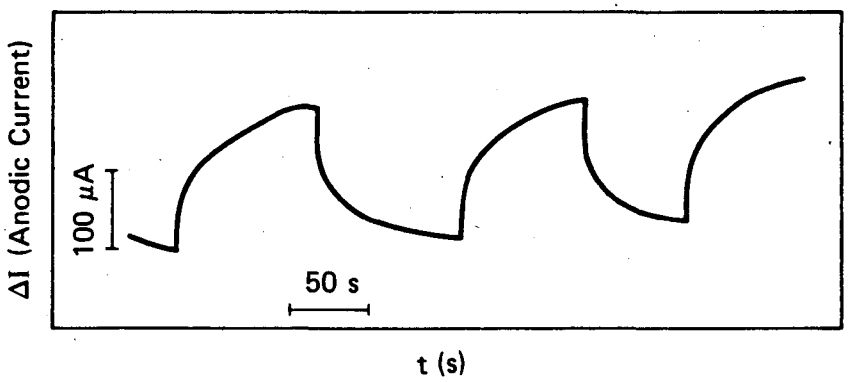

JA-350583-89

FIGURE 14 PHOTOCURRENT (ΔI) AS A FUNCTION OF TIME AT CONSTANT POTENTIAL (+1.25 V vs SHE).

Solution: 0.1 N $NiSO_4$, 0.1 N NaAc, 0.001 N KOH (Briggs solution) F-type film

IMPEDANCE MEASUREMENTS ON NICKEL ELECTRODES

Impedance measurements on native NiO electrode films in strong alkali are reported here as a function of frequency and applied potential. We show that the reduced film is potential dependent but that the oxidized is not. Glarum and Marshall (2) recently published similar findings, but in our work, we analyzed the data in terms of the semiconductor properties of the Ni(II) oxide film.

Figure 15 shows a typical Nyquist plot for the discharged electrode (-0.32 V vs SHE). By expanding the high-frequency region of this plot (see Figure 16), we see that it exhibits two semicircles. At more negative applied dc bias, the two semicircles become increasingly well resolved. At a more positive dc bias, the first semicircle gradually merges with the second; this is clearly illustrated for the charged electrode in Figure 17 (+0.61 V vs SHE), in which case only the onset of one semicircle is to be seen. This same figure also illustrates that the Nyquist plot described a diffusional process (45° angle), whereas the first semicircle in Figure 16, for example, describes a single R-C parallel combination (90° angle).

The above is even more evident when observing a Bode plot at, for example, -0.785 V vs SHE, as shown in Figure 18. In the frequency range of the first semicircle in a Nyquist plot, the corresponding Bode plot exhibits a slope approaching -1 (capacitive behavior, phase -90°). In the region of the second semicircle, the slope is close to -1/2 (diffusional process, phase -45°). The more positive the voltage at which the impedance measurements were made, the more the region with slope -1/2 prevails. The Bode plot corresponding to the Nyquist plot shown in Figure 17 shows only one line with slope -1/2, and the phase is -45° over the whole frequency range (see Figure 19). The origins of these different processes are considered separately.

The first semicircle, which is best resolved in the discharged region, can be attributed to a simple R-C circuit, with C the capacitance of the space charge layer of the Ni(II) oxide film and R the interfacial reaction, charge transfer resistance. In the discharged region, the NiO electrode shows a much smaller capacitance than in the charged region. Moreover, this small capacitance is voltage dependent, whereas the capacitance measured for the charged electrode is voltage independent. This is illustrated in Figure 20, which shows a plot of X^2 vs V at 1000 Hz (X = imaginary component of the impedance): at 1000 Hz, we can say to a good approximation that $X = -1/\omega C$.

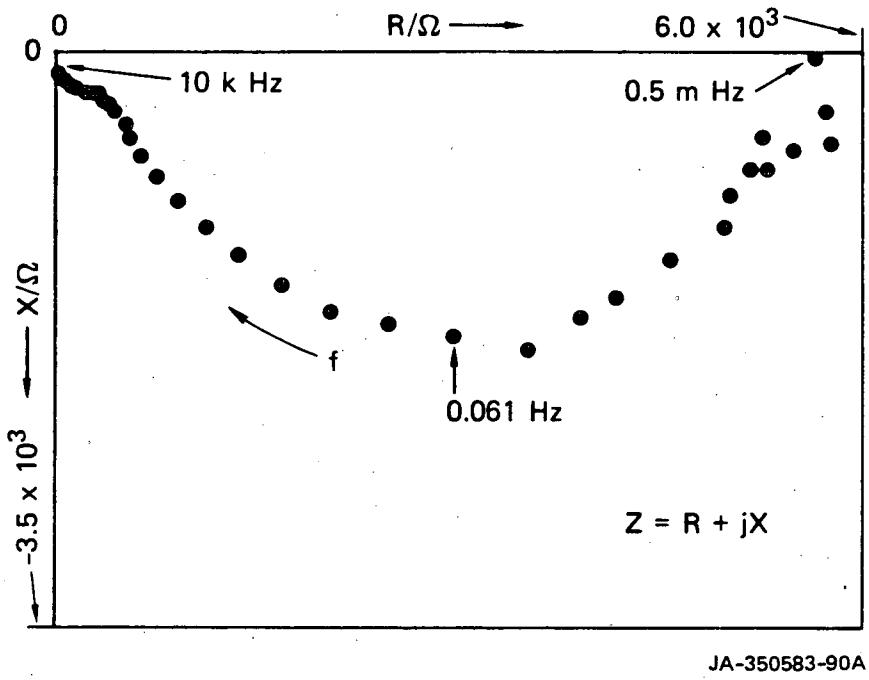

FIGURE 15 NYQUIST PLOT FOR APPLIED POTENTIAL OF -0.32 V vs SHE

Solution: 5 N KOH. Surface area: 0.452 cm^2.

From semiconductor theory, we expect that in the presence of a space charge, the voltage dependence of the capacitance of that space charge will follow a Mott-Schottky relationship. This relation is given by

$$\frac{1}{C^2} = \frac{2}{eN_A\epsilon_o\epsilon_A}\left(-V + V_{FB} - \frac{kT}{e}\right) \text{ (for a p-type)}$$

$$\frac{1}{C^2} \sim V \text{ (and thus } X^2 \sim V) \quad .$$

In this formula, N_A is the acceptor density in the semiconductor, V_{FB} is the flatband potential, ϵ_A is the dielectric constant of the semiconductor, and ϵ_o is the dielectric constant in vacuum. The linear portion of a plot of the X^2 as a function of V might indicate that space charge effects indeed play some role in the impedance behavior of the discharged nickel oxide electrode.

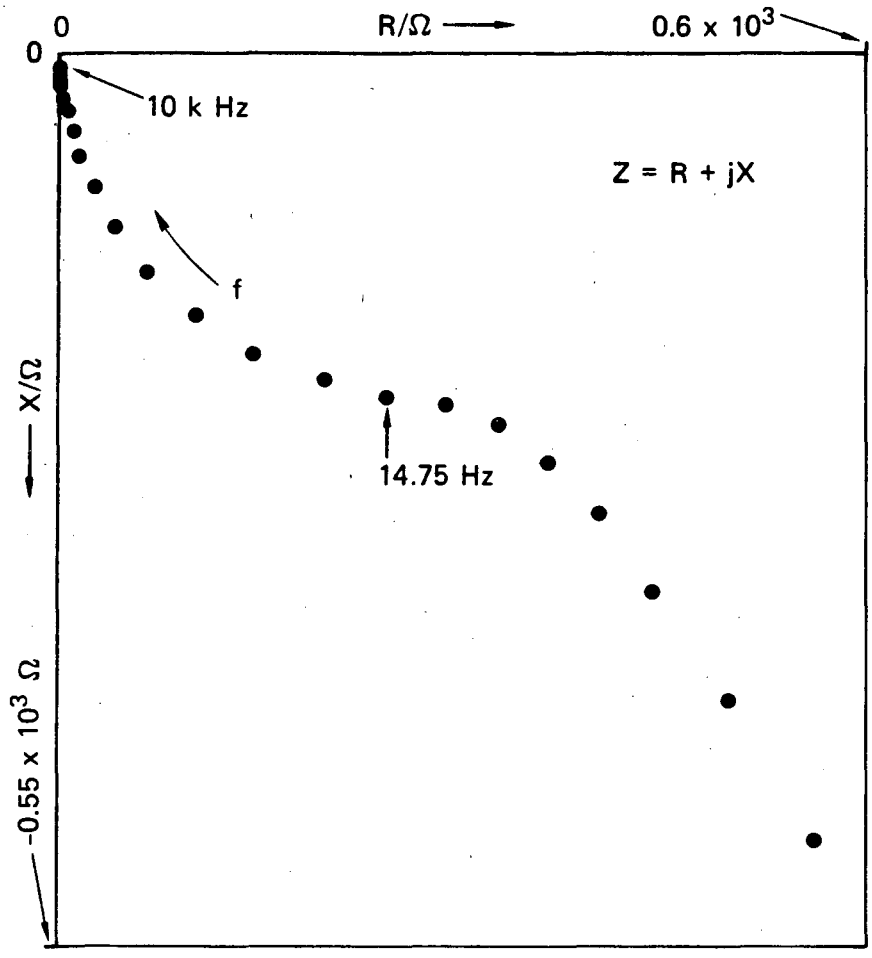

JA-350583-91A

FIGURE 16 EXPANDED NYQUIST PLOT FOR APPLIED POTENTIAL OF -0.32 V vs SHE

Solution: 5 N KOH. Surface area: 0.452 cm^2.

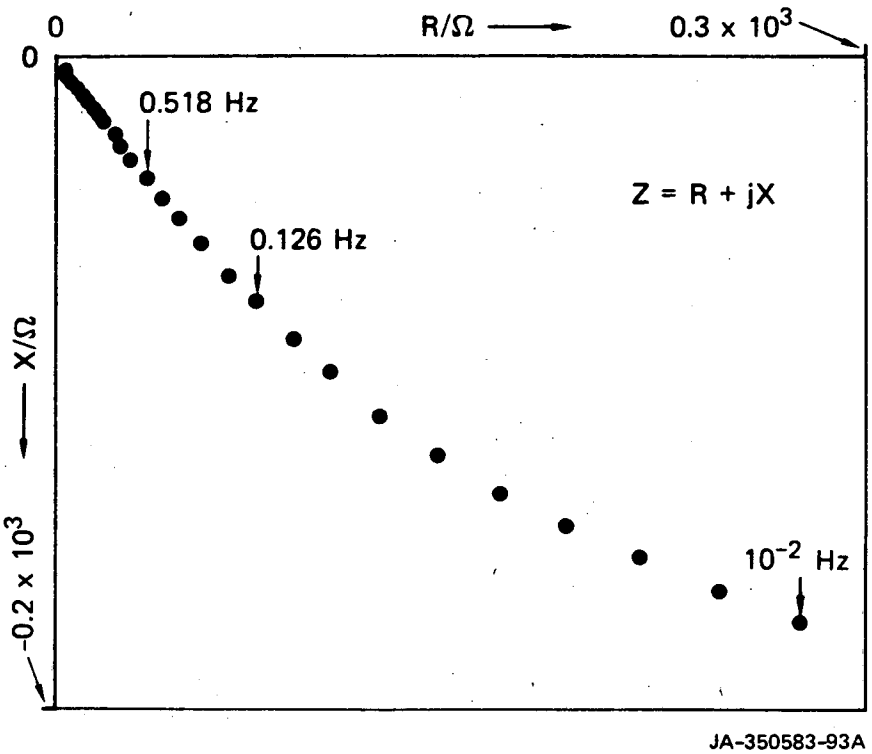

FIGURE 17 NYQUIST PLOT FOR APPLIED POTENTIAL OF +0.61 V vs SHE

Solution: 5 N KOH. Surface area: 0.452 cm^2

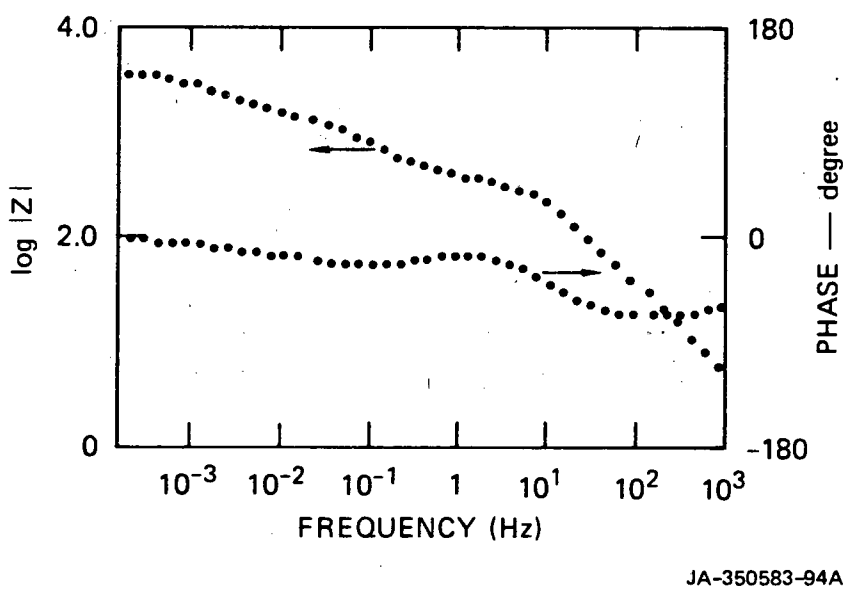

FIGURE 18 BODE PLOT FOR APPLIED POTENTIAL OF -0.785 V vs SHE

Solution: 5 N KOH. Surface area: 0.452 cm^2

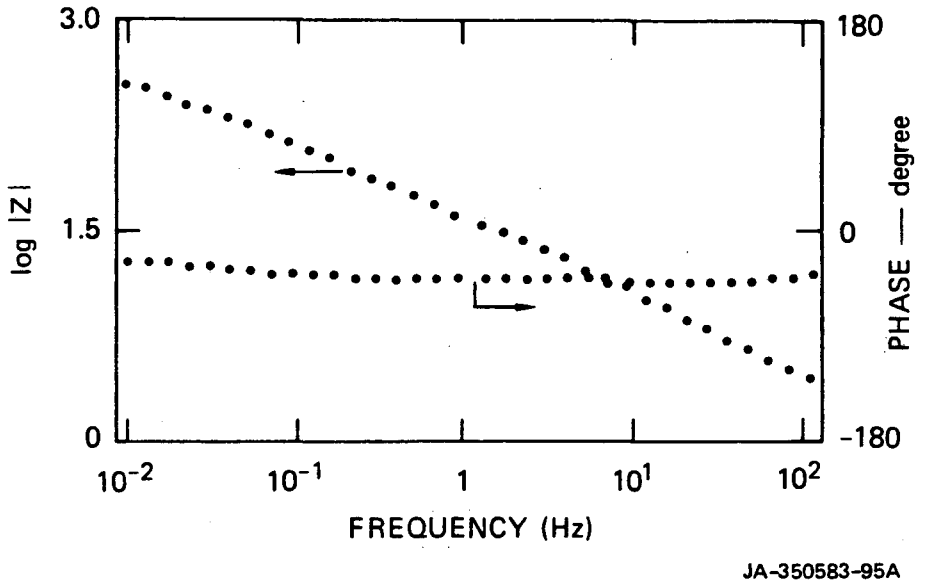

FIGURE 19 BODE PLOT FOR APPLIED POTENTIAL OF +0.614 V vs SHE

Solution: 5 N KOH. Surface area: 0.452 cm^2

The flatband potential determined in 35 wt% KOH for our electrodes was +0.100 V vs SHE. Work on crystalline NiO by Tench and Yeager (26) suggests the following expression for the flatband potential of their highest doped material as a function of pH:

$$V_{FB} = 1.490 - 0.100 \text{ pH} \quad .$$

Assuming a pH of 14.5 for the solution used in the experiment described in Figure 20, we predict on the basis of this formula that

$$V_{FB} = -0.040 \text{ V vs SHE} \quad .$$

The correspondence with our value of -0.100 V for V_{FB} is remarkably good in view of the approximations and extrapolations involved in obtaining V_{FB}. However, both values are only in fair agreement with the 0.215 V vs SHE for V_{FB} calculated with the expression given by Rouse and Weiniger (28)

$$V_{FB} = 0.94 - 0.050 \text{ pH} \quad .$$

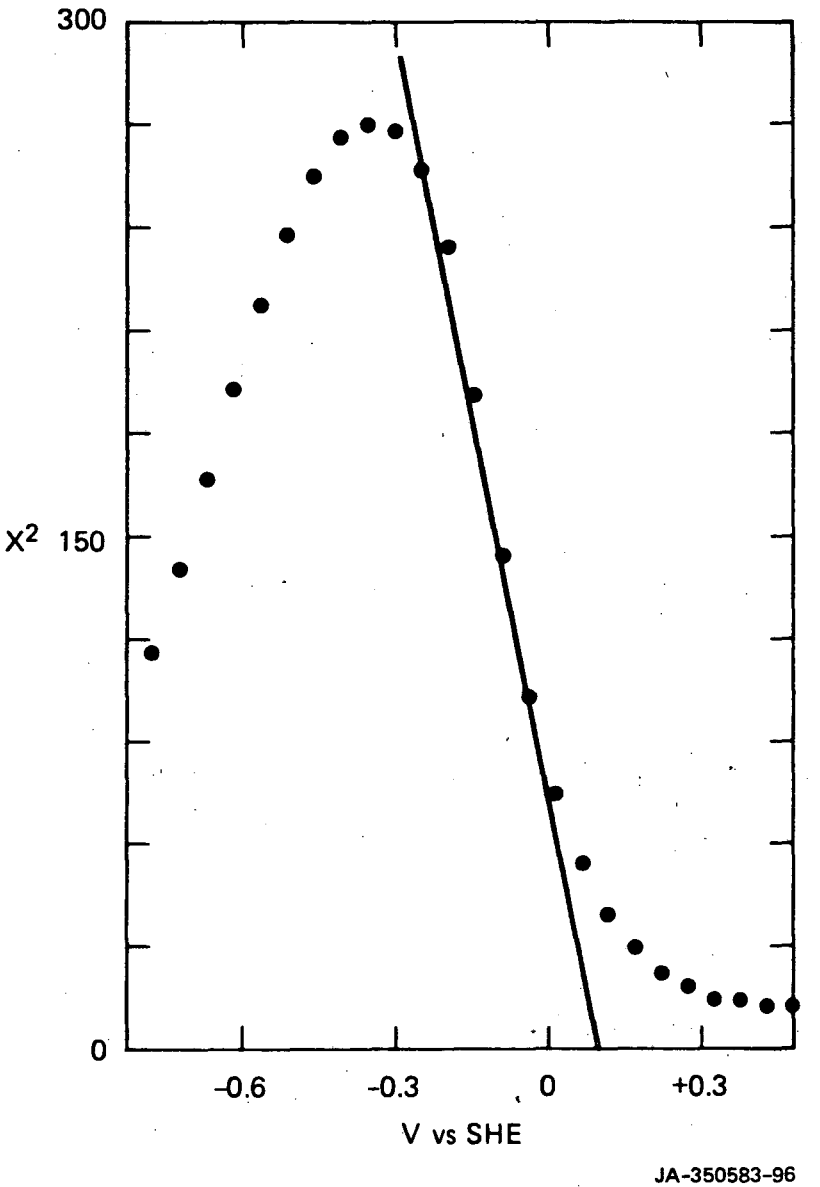

FIGURE 20 PLOT OF X^2 vs V vs SHE FOR A Ni ELECTRODE IN 35 wt% KOH

$X = 1/2\ \pi\ f\ C$, f = 1000 Hz.

The shortness of the voltage range over which the depletion region governs the impedance behavior presumably has to do with the high doping level of the oxide. This is already obvious from the relatively high capacitance for the NiO even in depletion. At high doping levels, tunneling through the space charge layer is likely to occur at relatively low reverse bias, at which point the Mott-Schottky relation breaks down. An extensive discussion of the potential distribution across a highly doped NiO/electrolyte interface was given by Tench and Yeager (26). It turns out that their theoretical predictions for a highly doped material such as studied here indicate that only at extremely large cathodic potentials (< -2 V vs V_{FB}), all the potential change occurs across the space charge region, and only in this potential range can linearity be expected in the $1/C^2$ vs V plot. The fact that, despite this, a linear $1/C^2$ vs V was observed at much less negative potentials (as observed in their work and the present study) they explain by the effect of specifically adsorbed cations, for example, H^+, which cause an exhaustive depletion layer to exist by strongly repelling the p-carriers (Ni^{3+}). The slope of the Mott-Schottky plot was not influenced by the presence of LiOH in the alkaline electrolyte. This tends to suggest that the influence of Li^+ is not to increase the conductivity of the discharged nickel electrode, as had been suggested by Tichnor to (8) explain improved battery operation in the presence of LiOH.

Ideally, the photocurrent onset at an intensely illuminated nickel electrode should correspond to the flatband potential. Thus we have another independent means of checking whether we are measuring a true flatband potential with our Mott-Schottky plots. Angelini et al. (12) report that the electrode potential corresponding to the reversal in sign of the photoeffect is in agreement with that reported by Rouse and Weiniger (28) for the NiO flatband potential. In a borate buffer of pH 8.7, they determined for the photoeffect sign inversion +0.55 V vs SHE; based on Rouse and Weiniger's expression for the flatband, +0.505 V vs SHE was expected. In 5N KOH and 35 wt% KOH solution, we found for the onset of the cathode photocurrent under high intensity illumination approximately +0.06 V vs SHE, corresponding well with the +0.10 V vs SHE we found for the flatband potential in 35 wt% KOH. As the pH decreases, we expect that the flatband potential and thus also the photocurrent onset shift toward more anodic values. Extrapolating our value for the photocurrent onset to the value expected in a solution of pH 8.7, we get either +0.590 V vs SHE [using the 0.100 V/pH slope given by Tench and Yeager (26)] or +0.325 V vs SHE [using the 0.05 V/pH slope given by Rouse and Weiniger (28)]. The former of the two values is close to +0.550 V vs SHE given by Angelini (12).

The concentration of the dopant can be calculated from the slope of the Mott-Schottky relation. In view of the above, the concentration is expected to be high. Taking into account a roughness factor of 1.5, we calculate an acceptor concentration of 4×10^{20} cm^{-3}. This is a very high doping level and represents almost the limit of applicability of the Mott-Schottky relation.

We propose that the nonstoichiometric, highly imperfect nature of the oxide film is responsible for its high conductivity. This doping level is almost the same as that reported by Tench and Yeager for their most highly doped material (2.4×10^{20} cm^{-3}). Both slope and intercept of our Mott-Schottky plots are acceptable and justify our assumption of the existence of a space charge in a cathodically polarized nickel electrode, which is also in accordance with the cathodic photocurrent in that potential region.

Because the impedance spectrum is observed to be independent of electrode rotation speed, the diffusional process responsible for the second semicircle in the Nyquist plot is most likely to be associated with the diffusion of ions within the oxide. Recently Zimmerman et al. (3) published impedance data on nickel-cadmium cells. Their results also pointed to solid-state diffusion in a surface film. Because their measurements were done on a NiCd cell, it was difficult for them to assign processes definitively, but an H^+ diffusion inside the NiO film was considered as a possible explanation for one of the two solid-state diffusion processes they describe. Assuming that the cell impedance is predominantly controlled by diffusion, σ, the Warburg coefficient can be determined from a plot of the impedance as a function of the square root of $\omega = 2\pi f$. The Warburg coefficient σ (29) can be represented by

$$\sigma = \frac{RT}{n^2 F^2 c_o \sqrt{2D}} ,$$

where c_o is the concentration of diffusing species and D is the diffusion coefficient. Zimmerman et al.(3) estimate the following values of $c_o\sqrt{D}$ for the two diffusion processes they assume: 1×10^{-7} mol cm^{-2} $s^{1/2}$ for process 1 and 1×10^{-6} mol cm^{-2} $s^{1/2}$ for process 2. From our data we calculate $c_o\sqrt{D}$ to be 5.7×10^{-9} mol cm^{-2} $s^{1/2}$, which indicates that process 1 is the solid-state diffusion inside the nickel oxide. The large discrepancy between our value and their value for $c_o\sqrt{D}$ is presumably due to the difference in dc current density in the respective experiments. The currents in our experiments were much smaller than in their experiments and a larger σ or smaller $c_o\sqrt{D}$ can be anticipated, as explained in Ref. (3); the equation for σ suggests that this might be because the concentration of diffusing species increases as current is increased, which is consistent with these species being either produced or consumed in the charge-transfer reactions. In the section entitled "Cyclic Voltammograms in the Dark," subsection "Untreated Nickel Electrodes," we deduced from a plot of i_p vs $\gamma^{1/2}$ a value of 5.5×10^{-8} mol cm^{-2} $s^{1/2}$ for $c_o\sqrt{D}$. Our two different methods give us values that are off by exactly a factor of 10.

Following Gerischer's approach (30), we now discuss the thermodynamic feasibility of the proposed photoreduction of Ni(II) oxide. For a reductive decomposition of a semiconductor to be possible, the associated decomposition energy must fall within the bandgap of the material. The same holds for the anodic decomposition of the material. First, we

construct an energy diagram for the Ni(II) oxide electrode. Unfortunately, data on flatband potentials--necessary to construct such a diagram--are scarce and somewhat contradictory. Since our value for the flatband potential was close to the value predicted by using the formula $V_{FB} = 1.490 - 0.100$ pH derived from Tench and Yeager's work(26), we use this value to construct the energy diagram. Since the Ni(II) oxide electrode is very highly doped, we can let the Fermi level coincide with the top of the valence band, and since the bandwidth is supposed to be about 3.7 eV for NiO, the following energy diagram at pH = 14 (Figure 21) results. In this figure, $E_{c,cdc}$ is the cathodic decomposition energy for Ni(II) oxide. The standard potential found in the literature (31) for the reduction of Ni(II) oxide in the reaction

$$Ni + H_2O = NiO + 2H^+ + 2e^-$$

is 0.110 V vs SHE. The energy level corresponding to the above potential for oxidation of pH = 14 is indicated in the diagram as $E_{c,cdc}$. This level is well within the bandgap. Therefore, from a thermodynamic point of view, the cathodic reduction is possible, because electrons excited to the conduction band are above the $E_{c,cdc}$ level and can fall into that level, leading to the reductive decomposition of Ni(II) oxide. This reduction mechanism is impossible in the dark, because under that condition, there are no electrons in the conduction band. In that case, reduction of H^+ or Ni(II) oxide is possible only by polarizing the electrode far enough negative so that valence band electrons can tunnel to the empty H^+ or Ni(II) oxide levels. For a highly doped material, like the oxide under investigation here, this will readily occur. We have seen in our cyclic voltammograms (Figure 7) that there is indeed evidence for such an occurrence.

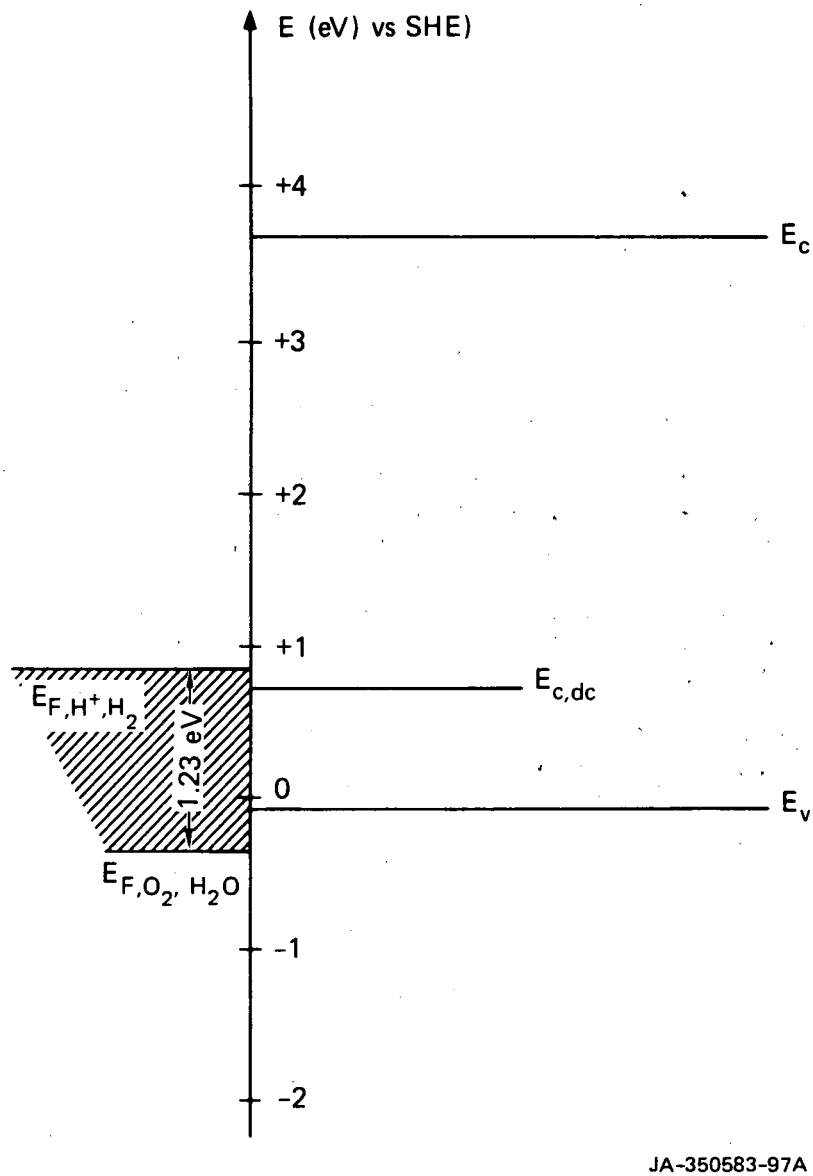

FIGURE 21 ENERGY DIAGRAM FOR Ni (II) OXIDE AT pH = 14 TOGETHER WITH FERMI-LEVELS FOR CATHODIC DECOMPOSITION ($E_{c,\ cdc}$), H^+/H_2 AND O_2/H_2O

EFFECT OF LITHIUM ADDITION

The beneficial effect of LiOH on the NiO electrode was discussed by Edison (32) in the first decade of the 20th century. In a nickel-iron cell, the addition of LiOH has a favorable effect on both the capacity and the life of the positive electrode. The presence of LiOH also influences the charge and discharge voltages. On discharge, a higher potential is initially observed. After a certain period of time, the poorer conductivity of the lithium-containing electrolyte counterbalances this effect, and the mean discharge potential is somewhat lower than when pure KOH electrolyte is used. On charge, the final potential increases with increasing amounts of LiOH.

The influence of LiOH on capacity, potential, and life of the NiO electrode has been discussed by several authors, and different theories have been put forward to explain the additive's effect. Foerster (33) suggested that LiOH maintains the positive active material in a finely divided condition by adsorption on the positive electrode. This would maintain the high surface area and thus the high capacity. Hofer (34) believed that strong surface adsorption of LiOH makes it possible to carry the nickel oxide electrode to a higher state of oxidation when charging. This theory would explain both the increase in capacity and the high initial discharge voltage.

Tichenor (8) explains the effect as a doping effect of NiO with lithium, affecting the extent to which the nickel active material can be oxidized or reduced.

Tuomi (9) also studied the effect of LiOH on the NiO material. He suggests that the oxidation of LiOH eliminates the γ-NiOOH phase:

$$Ni(OH)_2 \rightarrow \beta\text{-NiOOH} \rightarrow \gamma\text{-NiOOH} \quad ,$$

thereby leading to a stable capacity. Eliminating the γ-NiOOH phase also makes possible a rapid oxidation of $Ni(OH)_2$ throughout the compacted layers, resulting in an apparent increase in the oxygen overvoltage. (Tuomi pointed out that β-NiOOH is an n-type semiconductor.)

Weiniger (10) explains the Li^+ effect, as we saw in the section entitled "Introduction to the Kinetics of the Nickel Electrode in KOH With and Without LiOH," differently again. He assumes that Li^+

penetrates into the crystal lattice, preventing K^+ ions from doing so. The effect is an increase in oxygen overvoltage, because the recombination of adsorbed oxygen is hindered, allowing greater charge acceptance.

From the results in the section entitled "Impedance Measurements on Nickel Electrodes," we can now exclude the Tichenor (8) model; Mott-Schottky plots indeed did not reveal a significant increase in p-type doping of the NiO in the discharge region. In the section entitled "Effect of Additives on the Nickel Electrode," we discuss with experiments that reveal the influence of Li^+ on the nickel electrode behavior.

EFFECT OF ADDITIVES ON THE NICKEL ELECTRODE

Introduction

Weiniger (10) recently charted additives to the $Ni(OH)_2$ electrode that have been studied since 1958, as shown in Figure 22. The elements without circles or squares were studied before 1965. The circled elements, beryllium, silicon, and lead, were studied by Harivel and coworkers (35). Selenium was studied by D. Cripis (36). The most extensive research efforts have concentrated on the few elements that have proven to better the performance of the NiOH; cobalt and lithium, and, to some extent, zinc.

	I	II	III	IV	V	VI	VII	VIII
2	Li	(Be)	B					
3	Na	Mg	Al	(Si)				
4	K / Cu	Zn	Sc		As	Cr / [Se]	Mn	Fe Co
5	Rb / Ag	Cd		Sn	Sb	Mo		
6	Cs	Ba / Hg	RARE EARTH	(Pb)	Bi	W		

SOURCE: Ref. (10)

FIGURE 22 TESTS OF ADDITIVES TO $Ni(OH)_2$ REPORTED IN THE LITERATURE

By performing cyclic voltammetry and impedance measurements in the presence and the absence of various additives on single electrodes, we were able in our work to simplify the assignment of known battery phenomena to either one of the half cells. Furthermore, by comparing cyclic voltammograms on single crystal NiO, nickel electrodes, and thick

electrodeposited films of NiO on nickel, we were able to distinguish between bulk and surface effects. If, for example, the influence of additives in the case of $Ni(OH)_2$ is a surface effect, it can be enhanced by the use of film electrodes, which are very thin as contrasted to normal structures, in which bulk properties are more pronounced.

In the case of the electrodeposited film, we also incorporated the impurities in the film by adding additives to the electrodeposition solution. Although our results should be tested on realistic battery plates, it appears that manufacturing could benefit from some of our findings.

Table 3 summarizes the various additives tested on the different NiO electrode configurations.

N.B: A Hg/HgO electrode was used as reference electrode for the study of additives on the nickel electrode behavior. The potentials were not converted to SHE in the figures.

Table 3

TEST OF ADDITIVES TO VARIOUS TYPES OF NiO ELECTRODES

Additive	Bare Nickel Electrode	NiO		
		Single Crystal	(C-film)	Impurity Incorporated
21% or 18.1% KOH	*	*	*	*
Li	*	*	*	*
Co	*	*	*	*
Fe	*	*	*	*
Ba	*	*	*	*
Zn	*	*	*	*
Ni	*	*	*	*

Lithium

The effect of LiOH addition was already discussed in some detail in the section entitled "Effect of Lithium Addition." The series of voltammagrams in Figure 23 and Figure 24(a), (b), (c), and (d) do show dramatically the effects LiOH addition has on all types of NiO electrodes studied here.

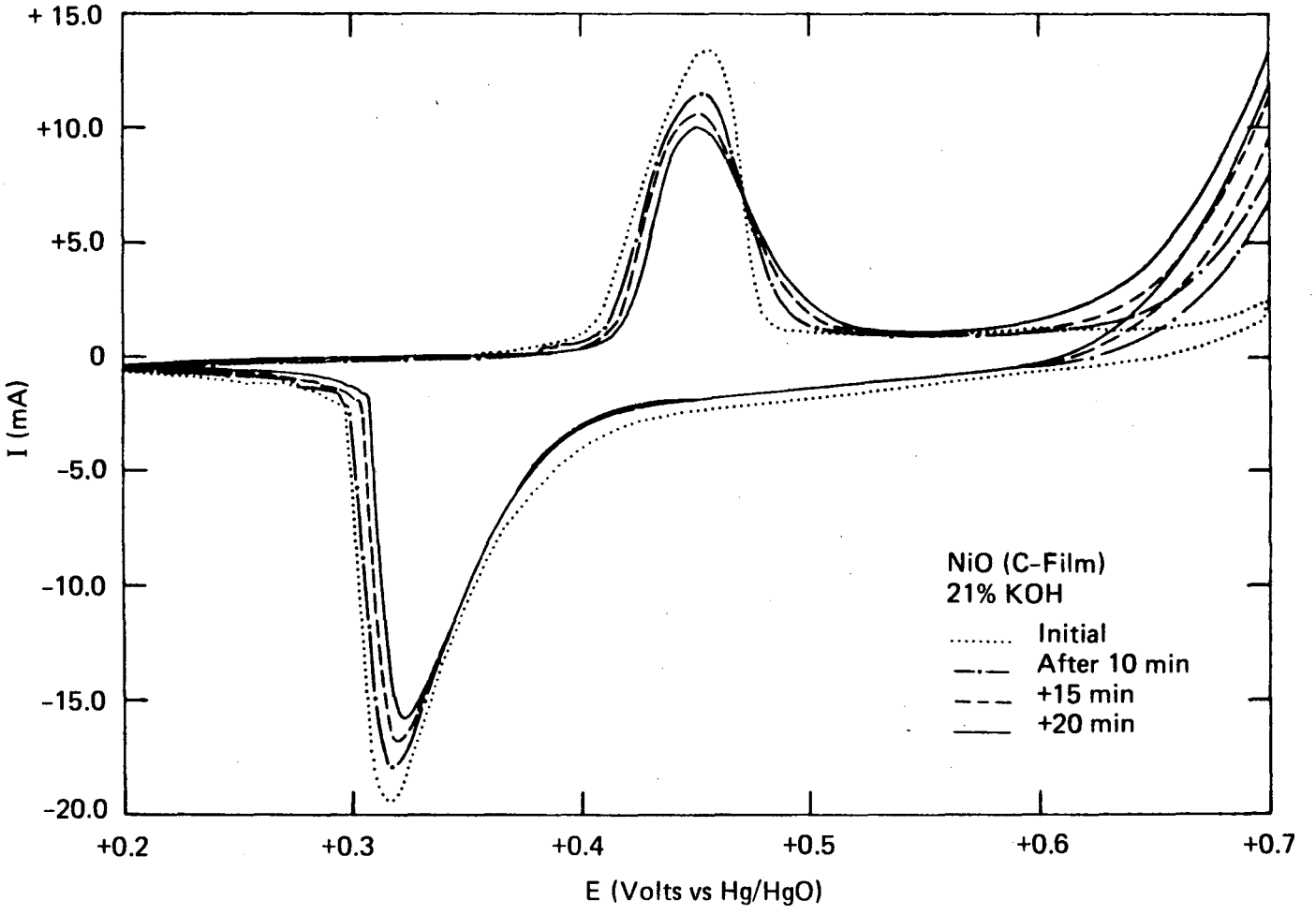

FIGURE 23 EFFECT OVER TIME OF LITHIUM ADDITIVE ON CYCLIC VOLTAMMOGRAMS FOR C-TYPE NiO FILM, 50 mV s^{-1}

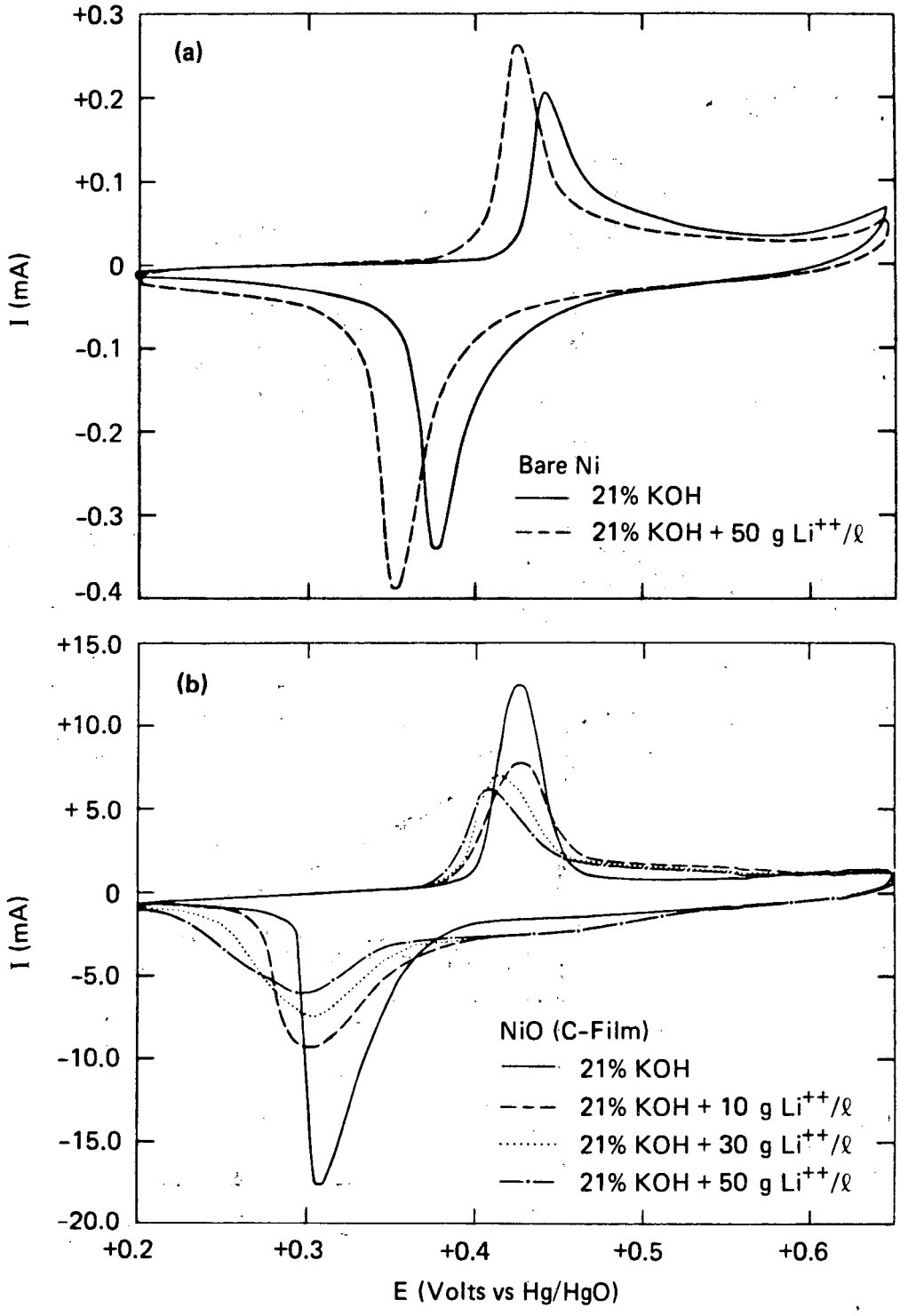

FIGURE 24 EFFECT OF LITHIUM ADDITIVE ON CYCLIC VOLTAMMOGRAMS, 50 mV s^{-1}

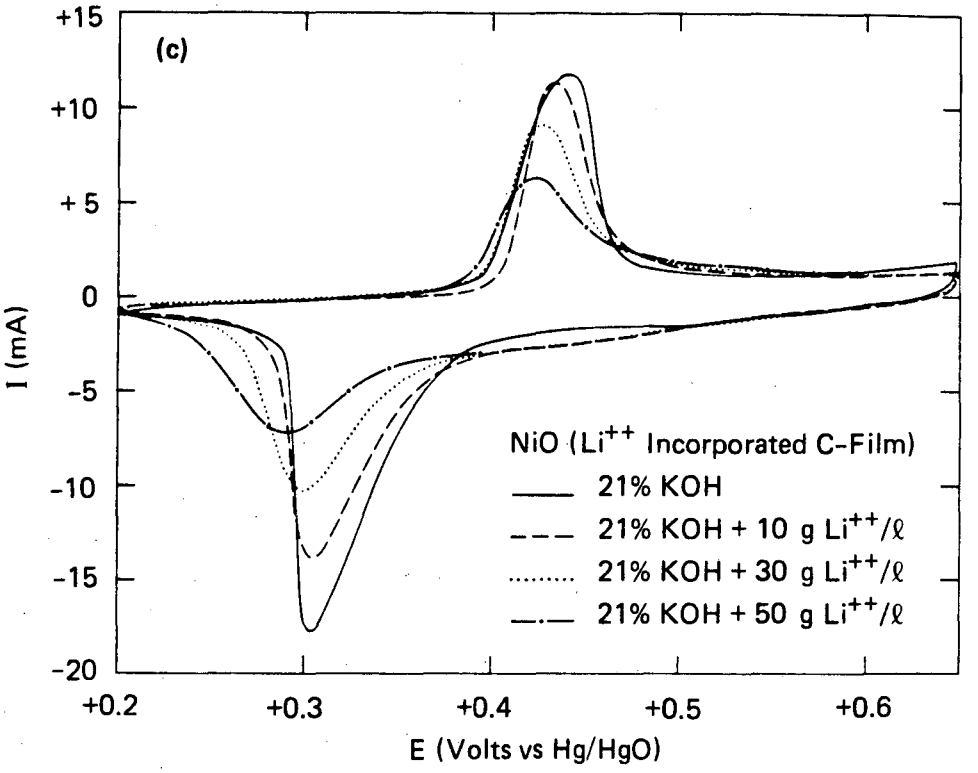

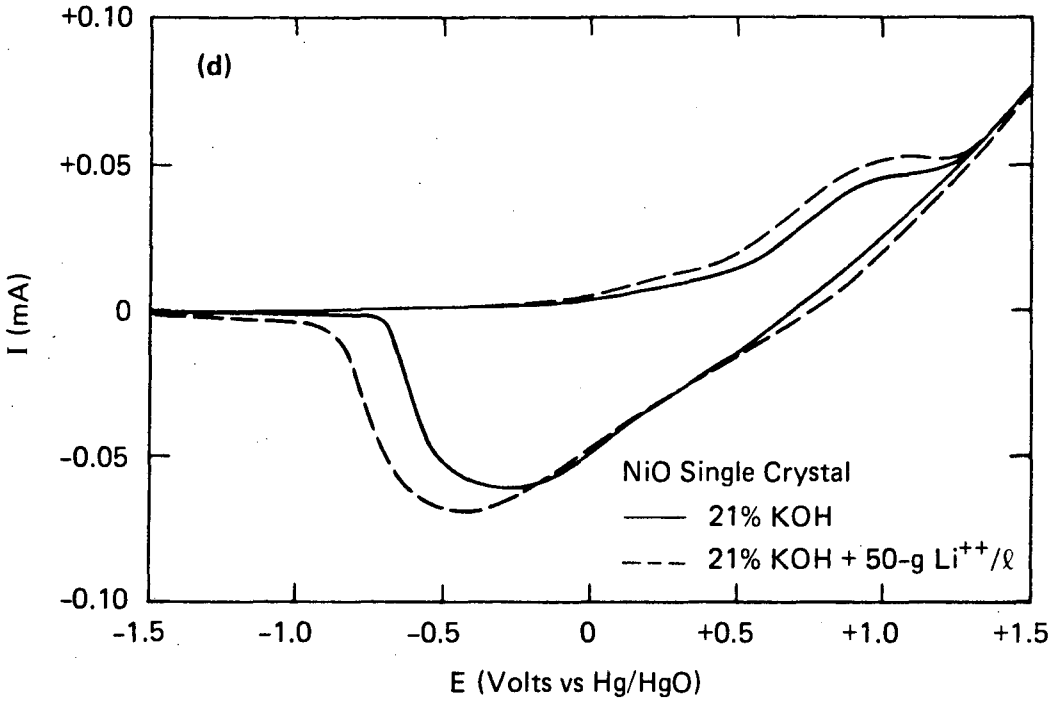

FIGURE 24 EFFECT OF LITHIUM ADDITIVE ON CYCLIC VOLTAMMOGRAMS, 50 mV s^{-1} (Concluded)

When the electrode is held in a 21 percent KOH solution at +0.2 V vs Hg/HgO for various times (0, 10, 15, and 20 minutes), a marked increase in the oxygen evolution is always noticed with both bare nickel electrodes and C-type NiO films; the effect is much less pronounced for the single crystal NiO. Figure 23 illustrates this effect for the C-type NiO film. When repeating the same experiment with the same timing, but with various amounts of LiOH added to the KOH, as shown in Figure 24(a), (b), and (c), that:

- The oxygen evolution rate is lower at the same potential.
- The oxygen evolution rate hardly increases at all as a function of time in the presence of LiOH.
- In all cases the charge/discharge peaks do shift cathodically (less overpotential), but the amount of charge decreases.

From Figure 24(d), it seems the oxygen evolution on a single crystal is hardly influenced and the charge/discharge peaks are changed very little. The diffusion of Li^+ in single crystal NiO is a very slow process, even at temperatures as high as 1500°C; it is thus very unlikely that we see Li^+ incorporation in the NiO lattice at room temperature. This indicates that the Li^+ effect is predominantly a bulk NiO lattice effect. Moreover in the sections entitled "Impedance Measurements on Nickel Electrodes," and "Effect of Lithium Addition," we gave experimental evidence that Li^+ does not increase the p-type conductivity of the discharged electrode. The above suggests that Weiniger's idea (10)--that Li^+ prevents K^+ from entering the lattice, thereby increasing the oxygen overpotential because the recombination of adsorbed oxygen is hindered--is the more likely explanation for the Li^+ effect. An incorporation of Li^+ in the crystal leads to the same electrode behavior [Figure 24(d)] as with the Li^+ in solution, suggesting that the Li^+ from solution is quickly incorporated in the NiO film, so that the two situations produce the same end result.

Iron

The amount of (II) and (III) valent iron in an alkaline battery electrolyte are normally quite low because of the very low solubility products of $Fe(OH)_2$ and $Fe(OH)_3$. The iron influence on cyclic voltammograms is illustrated in Figure 25(a), (b), and (c) and (d). Iron (III) valent ions were added under the form of the sulfate salt to a 21 percent or a 121 percent KOH solution. At a concentration of 10^{-3} molar the iron was not completely dissolved, so the solution was considered saturated.

It is obvious from Figure 25 that iron drastically decreases the overvoltage for oxygen for all electrodes. This is a detrimental effect for the battery, because increased oxygen evolution may prevent the interior of the nickel oxide in an actual battery electrode from becoming fully oxidized during constant current charging. It can also be observed [most clearly from Figure 25(a), (b), and (c) that the charging

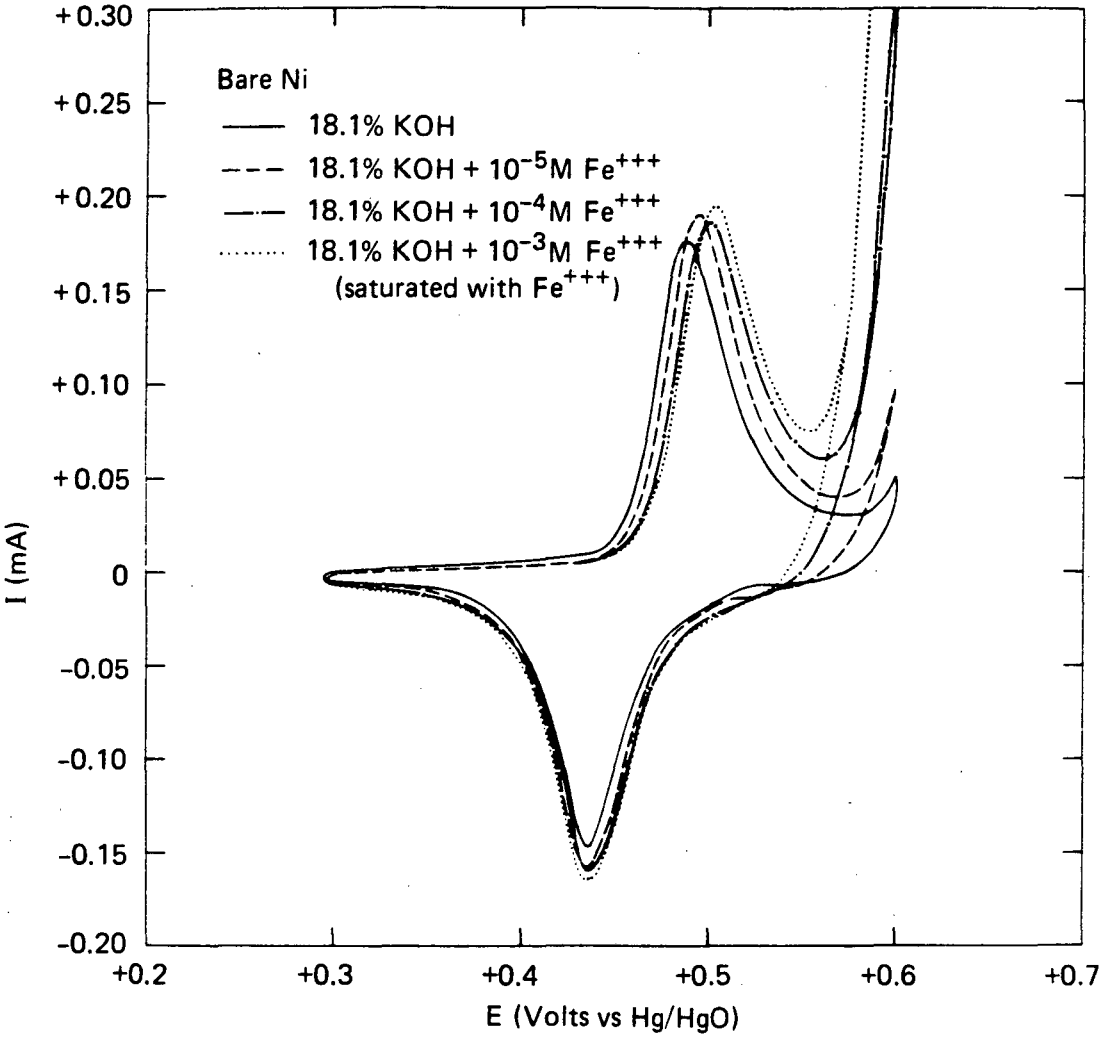

(a)

FIGURE 25 EFFECT OF IRON ADDITIVE ON CYCLIC VOLTAMMOGRAMS, 50 mV s^{-1}

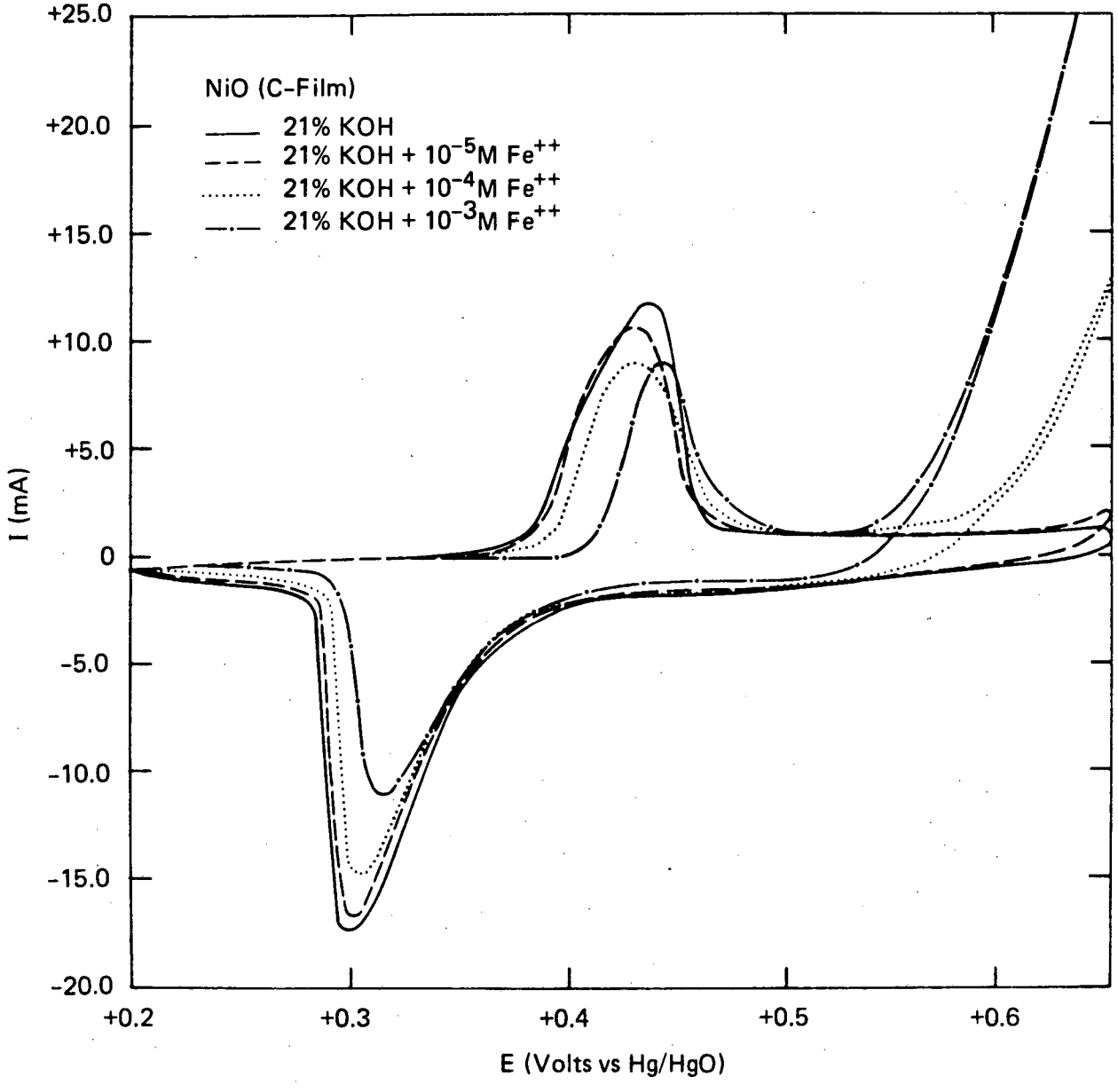

(b)

FIGURE 25 EFFECT OF IRON ADDITIVE ON CYCLIC VOLTAMMOGRAMS, 50 mV s^{-1} (Continued)

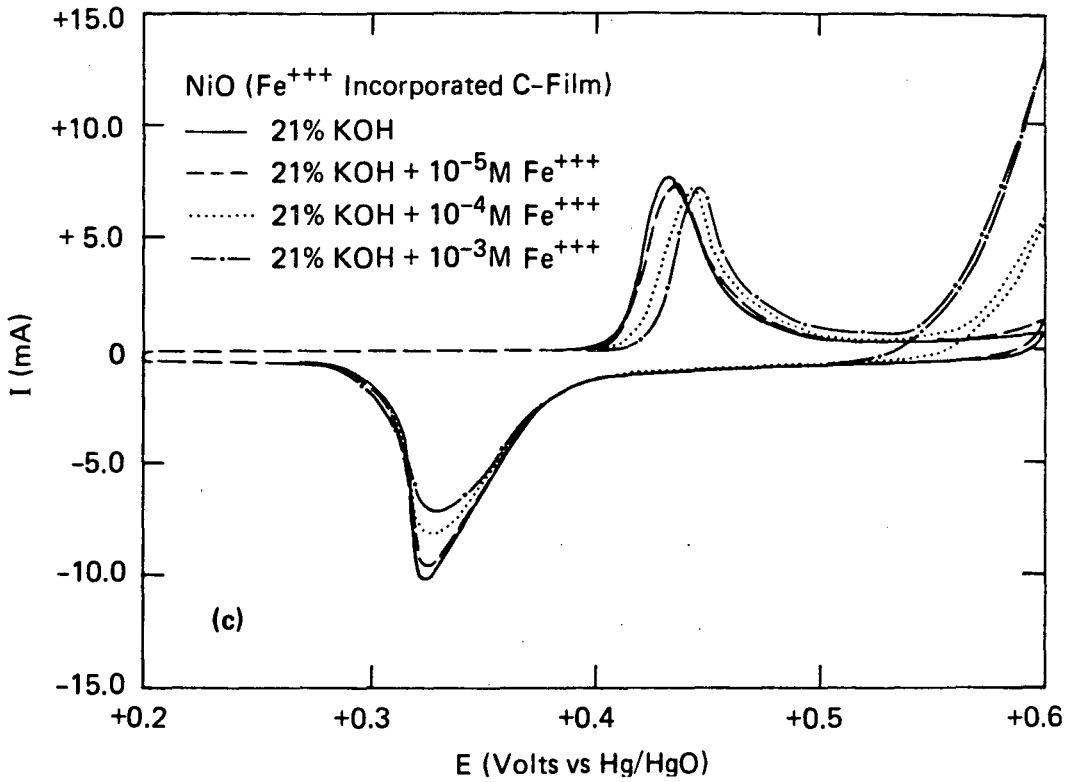

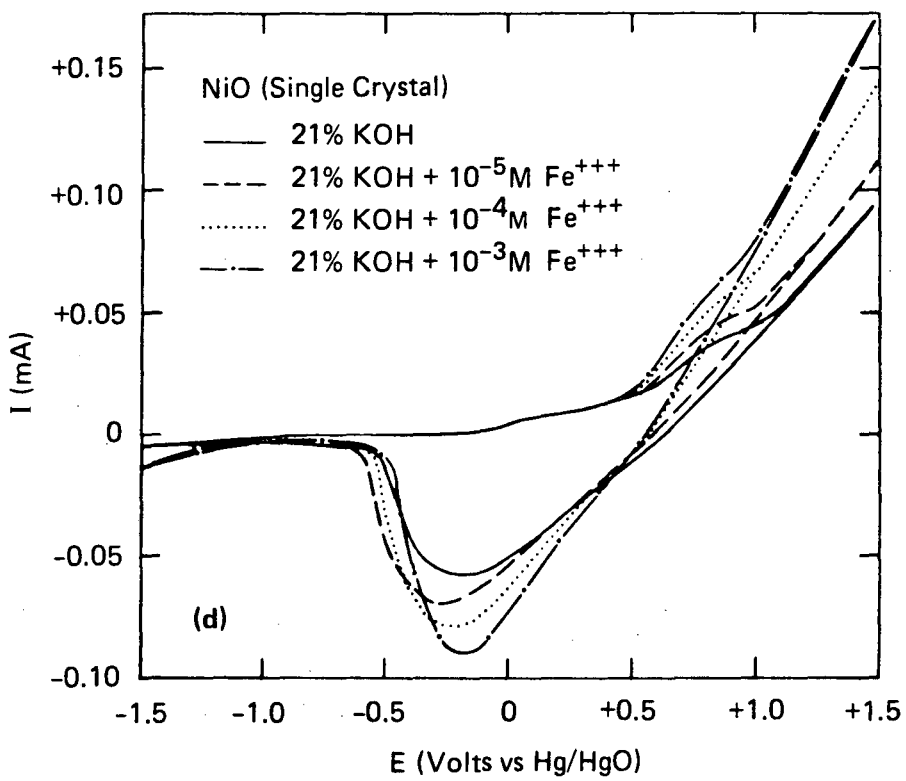

FIGURE 25 EFFECT OF IRON ADDITIVE ON CYCLIC VOLTAMMOGRAMS, 50 mV s^{-1} (Concluded)

peak shifts toward more anodic voltages with increased Fe^{++} impurity content in the electrodeposited film. Because the Fe^{+++} also increases the oxygen evolution rate of the single crystal NiO, we concluded that the Fe^{+++} is a surface effect only and, unlike the lithium effect, has little to do with the NiO crystallography. To determine whether the various waiting times before complete dissolution of the salts were responsible for the described phenomena, we tested the same waiting times before cycling but in a solution without iron addition. In this case, the effects described above were not observed.

Cobalt

Sintered NiOH electrodes, in general, require additives to obtain high efficiency, chemical stability, and long cycle life. The additive that is most commonly used is CoOH, which has been found to enhance cycle life and charging efficiency, and inhibit electrode growth. CoOH is in most respects an ideal additive, but because of its increasing scarcity and high cost, alternatives are being sought. If the mechanism could be understood, we might be able to select additives without trial and error testing of the complete table of chemical elements.

In battery manufacturing, cobalt in the form of $CoSO_4$ is added as a component in the positive active material preparation. The Ni:Co proportion is typically between 20:1 and 100:1 by weight. Weiniger (10) claims that the cobalt remains as Co^{+3} throughout the cycle life. By a combination of chemical, electrochemical, and X-ray analysis, Maladin and coworkers have shown (37) that the β form remains stable under conditions that in the absence of cobalt would give rise to γ-NiOOH. Even at overcharge, only small amounts of γ-NiOOH are formed. Thus the presence of Co^{+3} in the layer lattice prevents the tight incorporation of K^+ (γ-NiOOH), while the greater mobility of the K^+ ion in β-NiOOH leads to improved cycling behavior at the electrode.

The experiment series in Figure 26 illustrates the Co effect. (Co^{++} was added as sulfate salt.) From Figure 26(a) we can see a dramatic increase in capacity at concentrations higher than 10^{-4} (at which point Co^{++} starts to precipitate out on the nickel electrode). There is also much more current in the range between charging and oxygen evolution. This is also true for the C-type film; at concentrations higher than 10^{-4} M Co, a big increase in electrode capacity is observed [Figure 26(b)]. Incorporating the Co^{++} in the electrodeposited film has little effect on the cyclic voltammogram, and the addition of CO^{++} does not influence the cyclic voltamograms on a single crystal appreciably. Co^{++} like Li^+, seems to inhibit the rapid increase of oxygen evolution with time usually observed with electrodes in pure KOH. The above experiments clearly show why cobalt has a beneficial effect on battery performance.

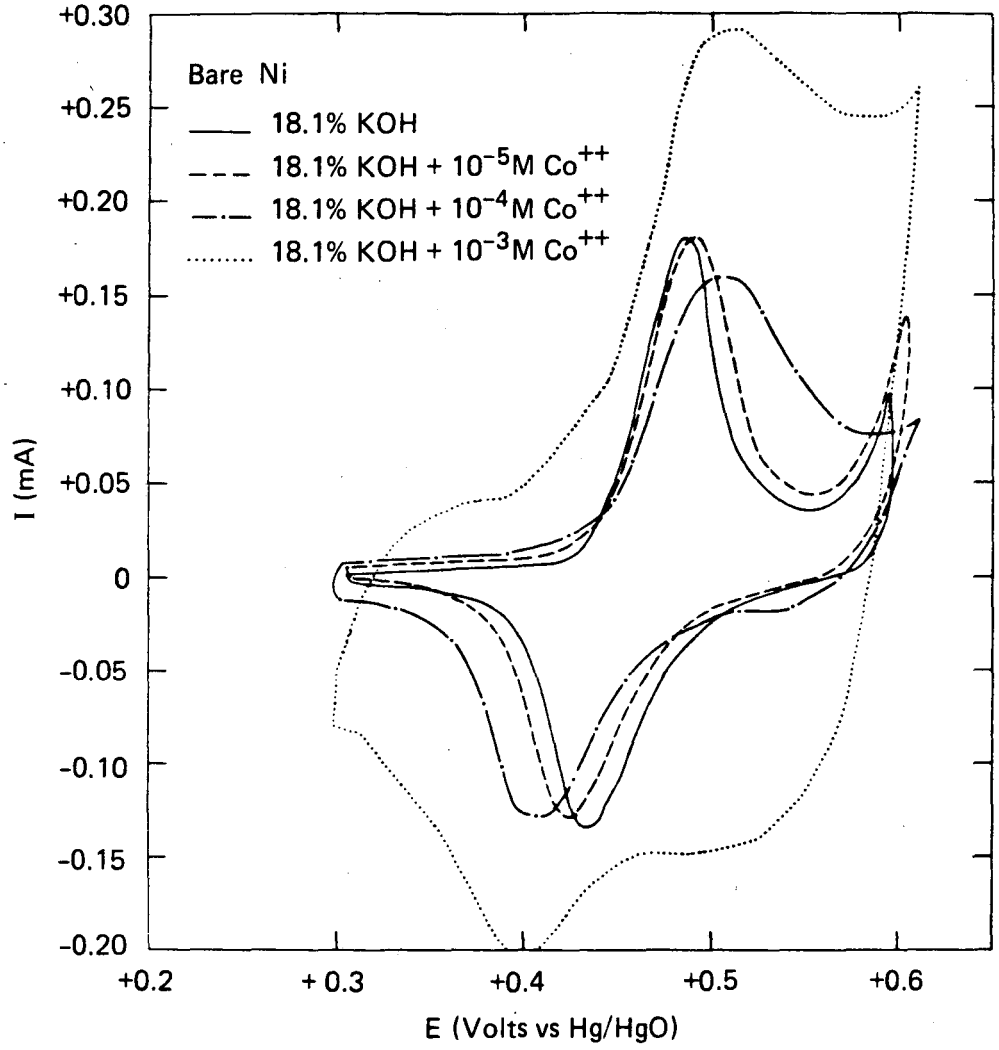

(a)

FIGURE 26 EFFECT OF COBALT ADDITIVE ON CYCLIC VOLTAMMOGRAMS, 50 mV s^{-1}

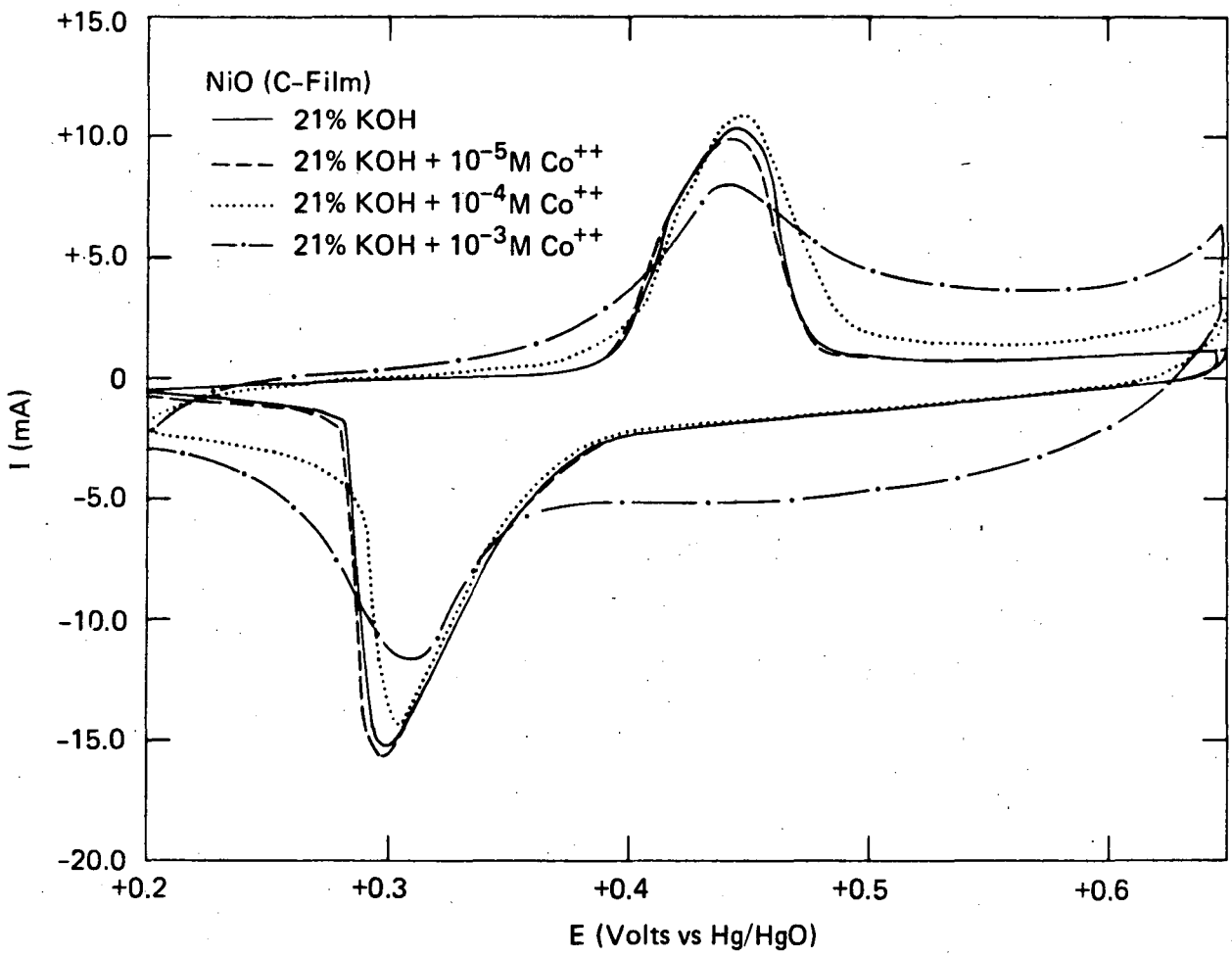

(b)

FIGURE 26 EFFECT OF COBALT ADDITIVE ON CYCLIC VOLTAMMOGRAMS, 50 mV s^{-1} (Continued)

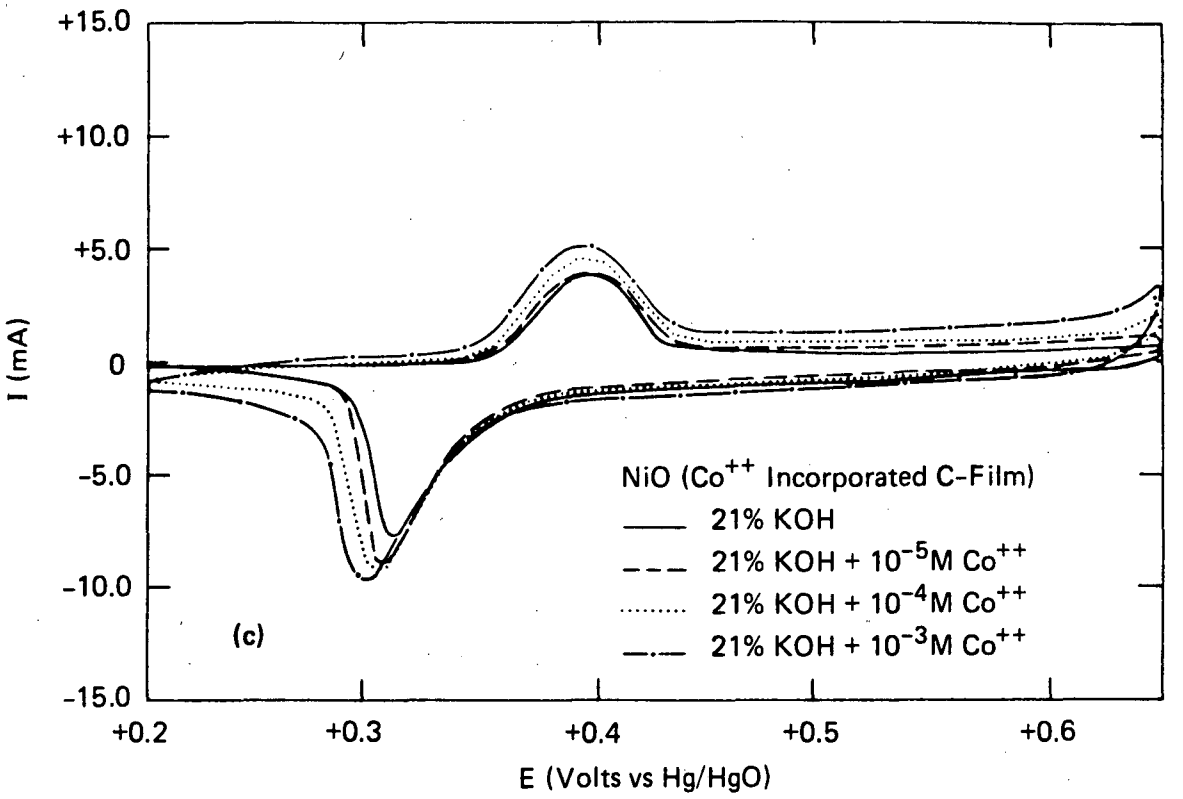

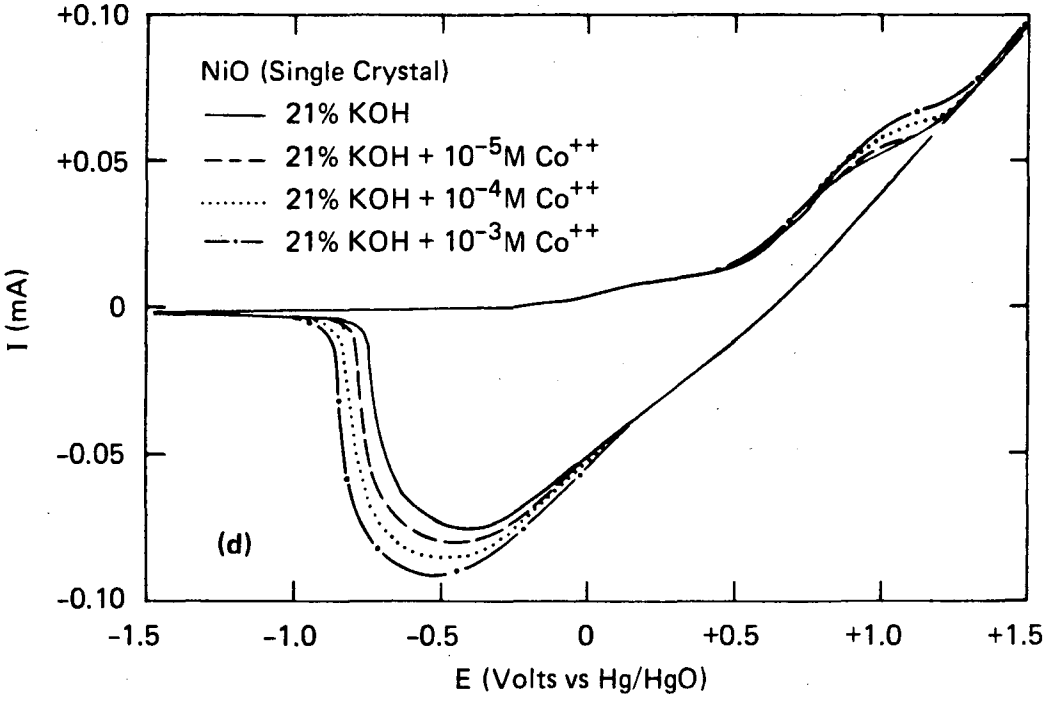

FIGURE 26 EFFECT OF COBALT ADDITIVE ON CYCLIC VOLTAMMOGRAMS, 50 mV s^{-1} (Concluded)

From Figure 26(d) it follows that the cobalt effect is not a simple catalytic effect, as is the iron effect. Comparing Figure 26(a) or (b) with Figure 26(c), it is evident that an addition of cobalt in solution is more effective than is incorporating the cobalt in the electrodeposited film.

Zinc

The concentration of zinc added to the alkaline solution was varied from 10^{-5} M Zn^{++} to 10^{-2} M Zn^{++}. On the bare nickel electrode we observed [Figure 27(a)] that the oxygen evolution increases with increasing Zn^{++} concentration; this is also the case for the single crystal NiO. In the case of the bare nickel electrode, we noticed that both charge and discharge peaks moved toward more anodic potentials with increasing Zn^{++} concentration. The discharge peak height also increased (increase in capacity).

In the case of the C-type film (with Zn^{++} added to the solution), the peaks do shift toward more anodic potentials, but the oxygen evolution is little influenced.

As with the Fe^{++}, the effect of zinc on oxygen increase is a surface effect and dominates for thin films. There is a noticeable increase in capacity, but overpotentials also increase [Figure 27(a)]. In more realistic structures in which bulk properties dominate (such as the C-type film), the increase in oxygen evolution is small and increase in capacity could be a major effect. We found the addition of Zn^{++} to be more effective when added to the cathode from the electrolyte than by codeposition. This impression was confirmed by Weiniger (38).

Barium

The effect of barium is illustrated in Figure 28(a), (b), (c), and (d). The oxygen overpotential is reduced for thin films but not to the extent that it is with Fe^{++}. There is some increase in capacity, but only for thin films. For all cases the discharge peak is shifted cathodically. Incorporation and solution-addition both seem to make yield the same results. More details will be reported in next year's annual report.

Nickel

The effect of nickel addition is being investigated in more detail now and will be discussed extensively (as will the barium-effect on nickel) in next year's report.

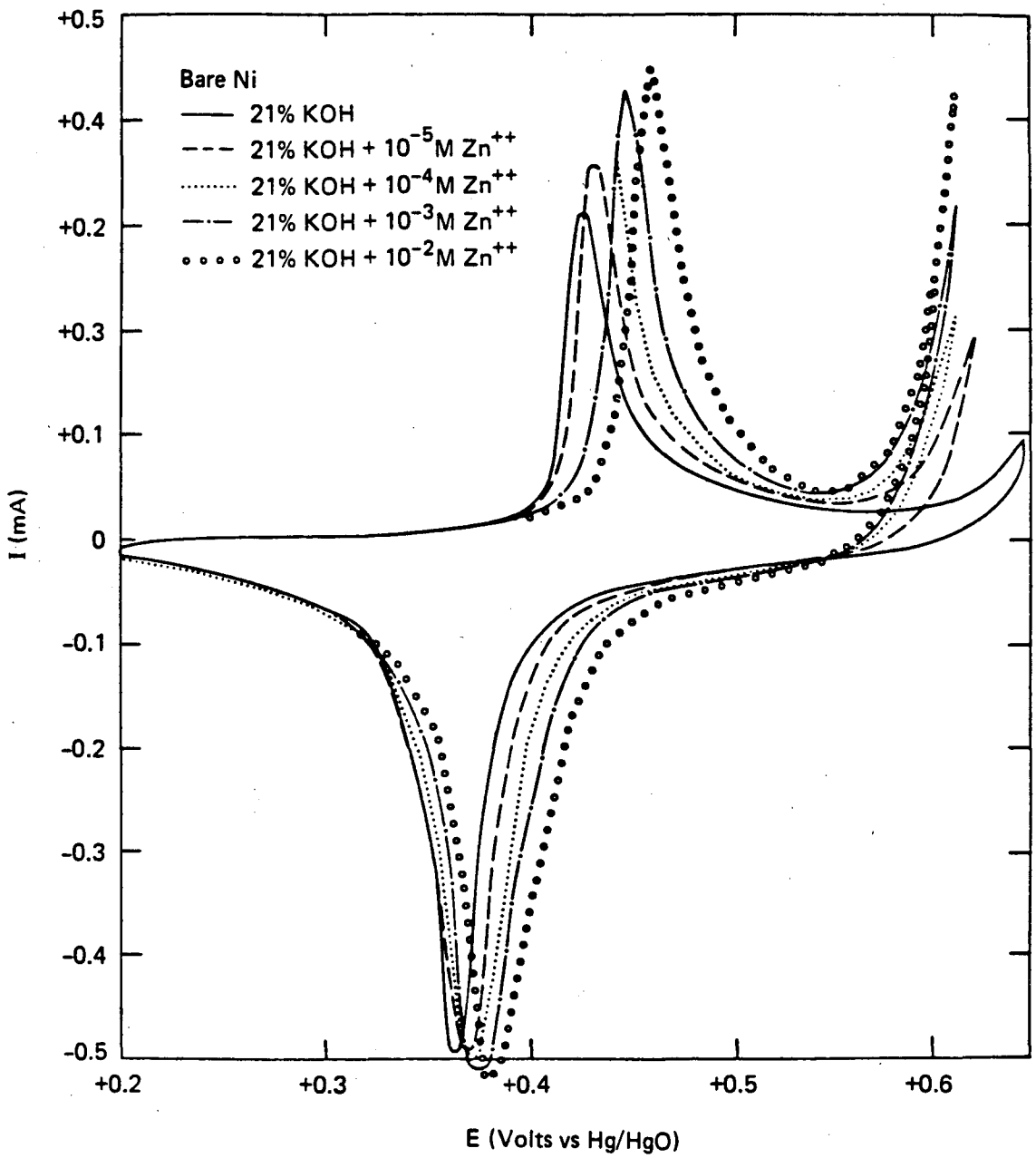

(a)

FIGURE 27 EFFECT OF ZINC ADDITIVE ON CYCLIC VOLTAMMOGRAMS, 50 mV s^{-1}

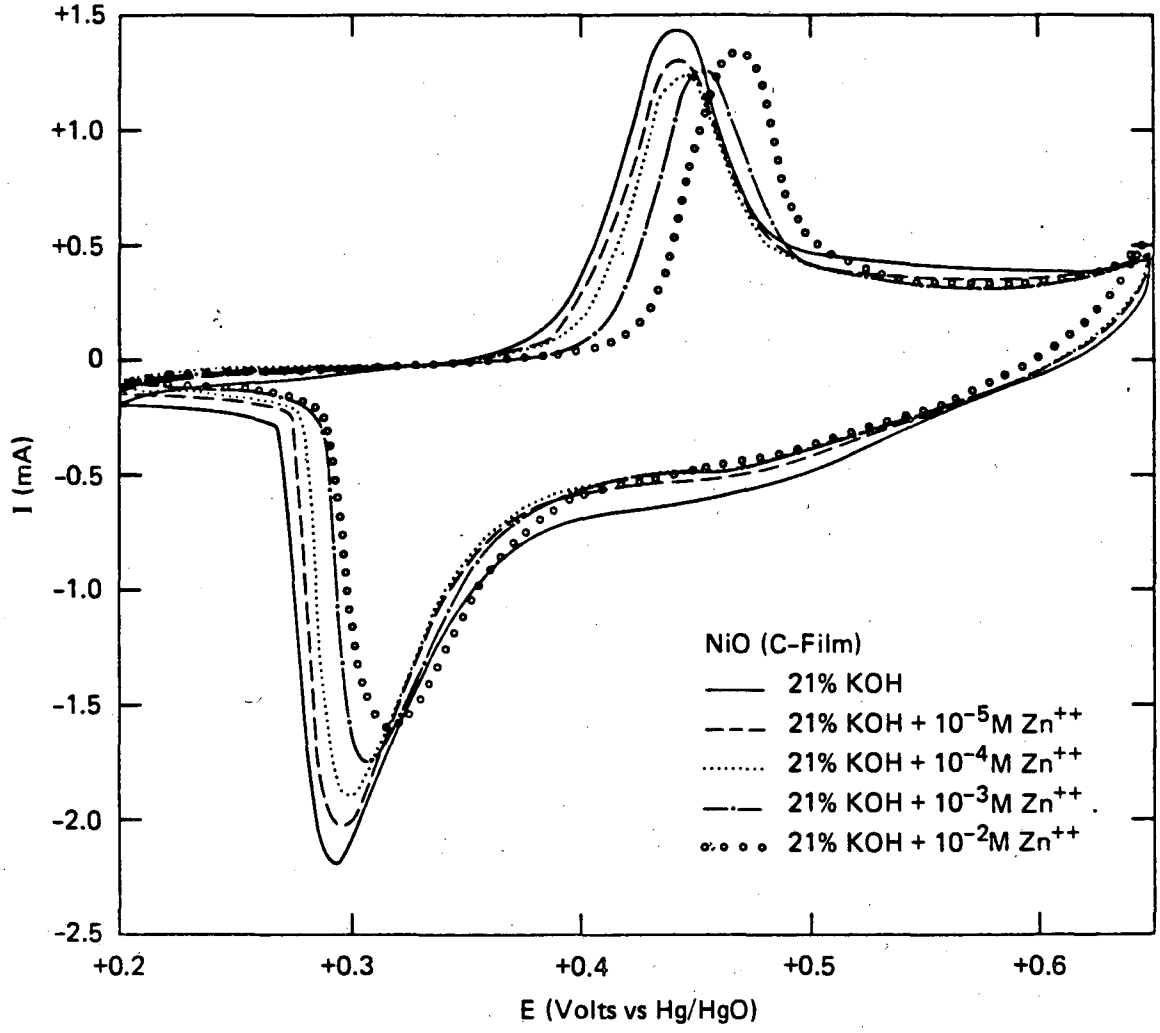

(b)

FIGURE 27 EFFECT OF ZINC ADDITIVE ON CYCLIC VOLTAMMOGRAMS, 50 mV s^{-1} (Continued)

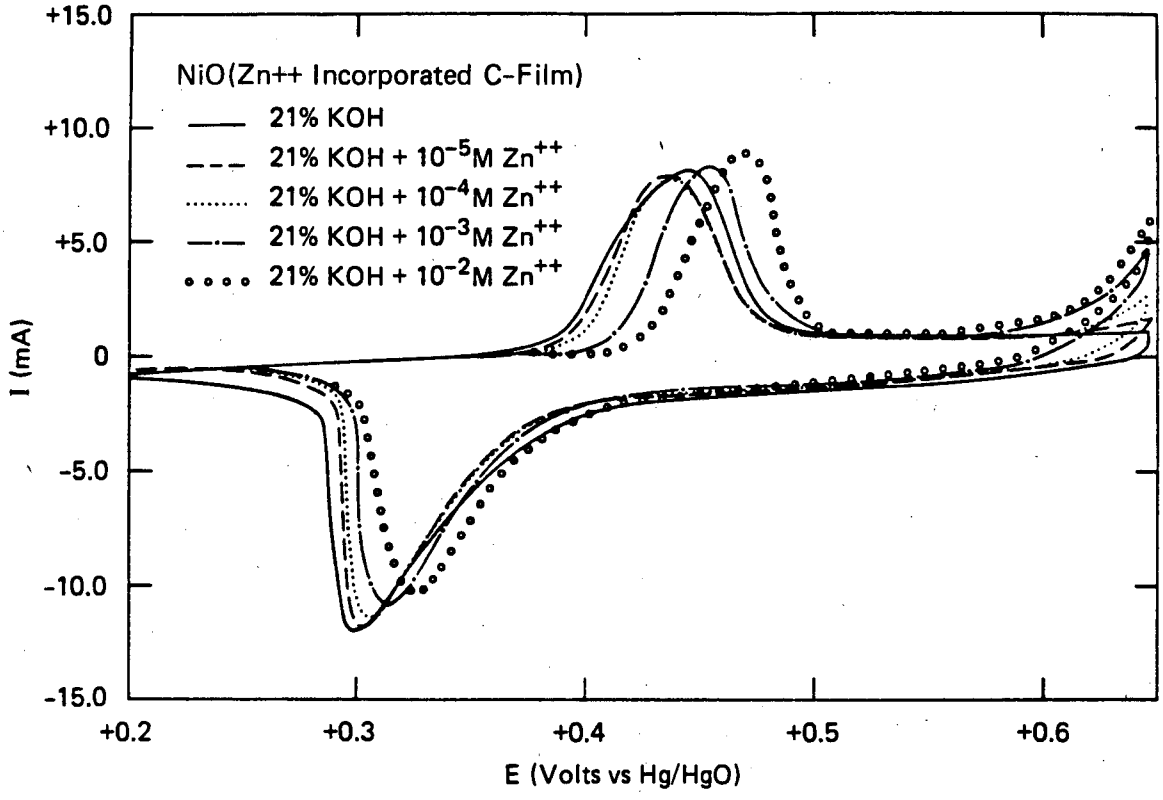

(c)

FIGURE 27 EFFECT OF ZINC ADDITIVE ON CYCLIC VOLTAMMOGRAMS, 50 mV s^{-1} (Continued)

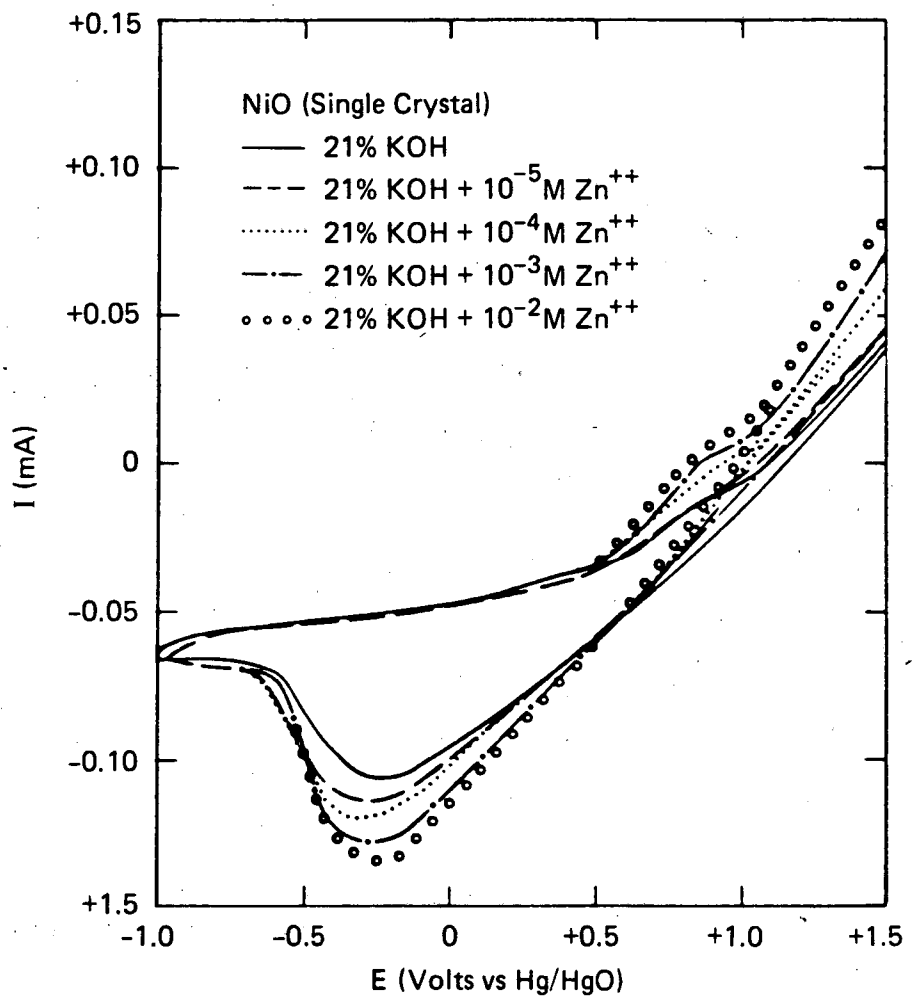

(d)

FIGURE 27 EFFECT OF ZINC ADDITIVE ON CYCLIC VOLTAMMOGRAMS, 50 mV s^{-1} (Concluded)

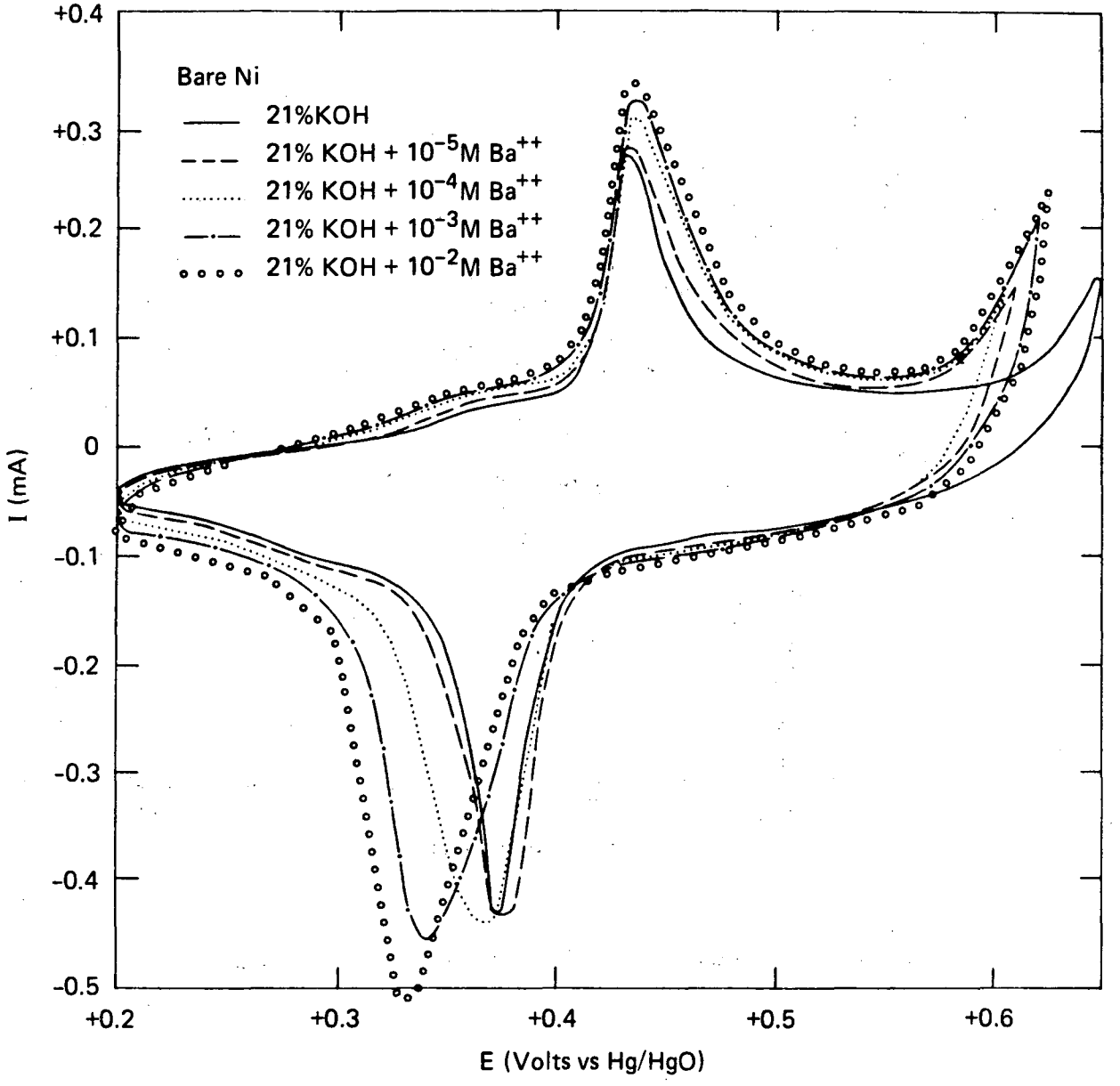

(a)

FIGURE 28 EFFECT OF BARIUM ADDITIVE ON CYCLIC VOLTAMMOGRAMS, 50 mV s^{-1}

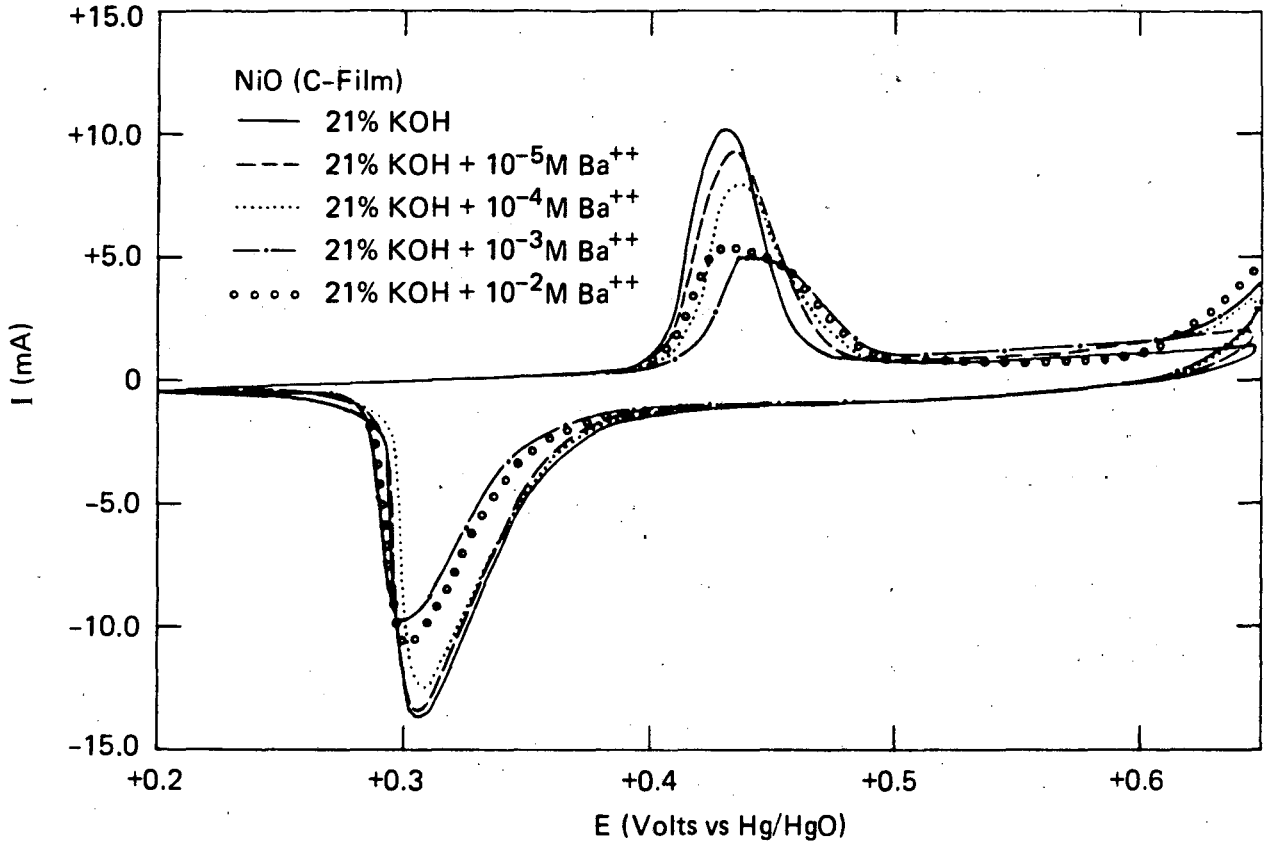

(b)

FIGURE 28 EFFECT OF BARIUM ADDITIVE ON CYCLIC VOLTAMMOGRAMS, 50 mV s^{-1} (Continued)

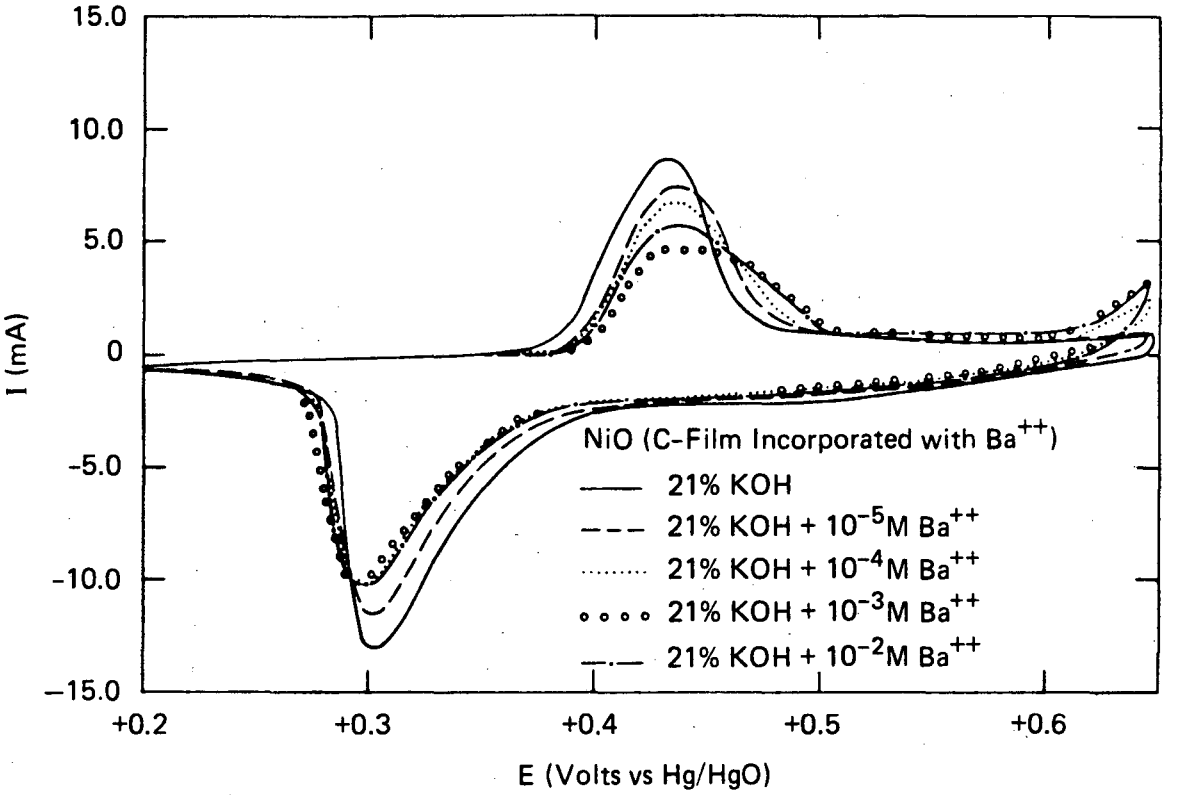

(c)

FIGURE 28 EFFECT OF BARIUM ADDITIVE ON CYCLIC VOLTAMMOGRAMS, 50 mV s^{-1} (Continued)

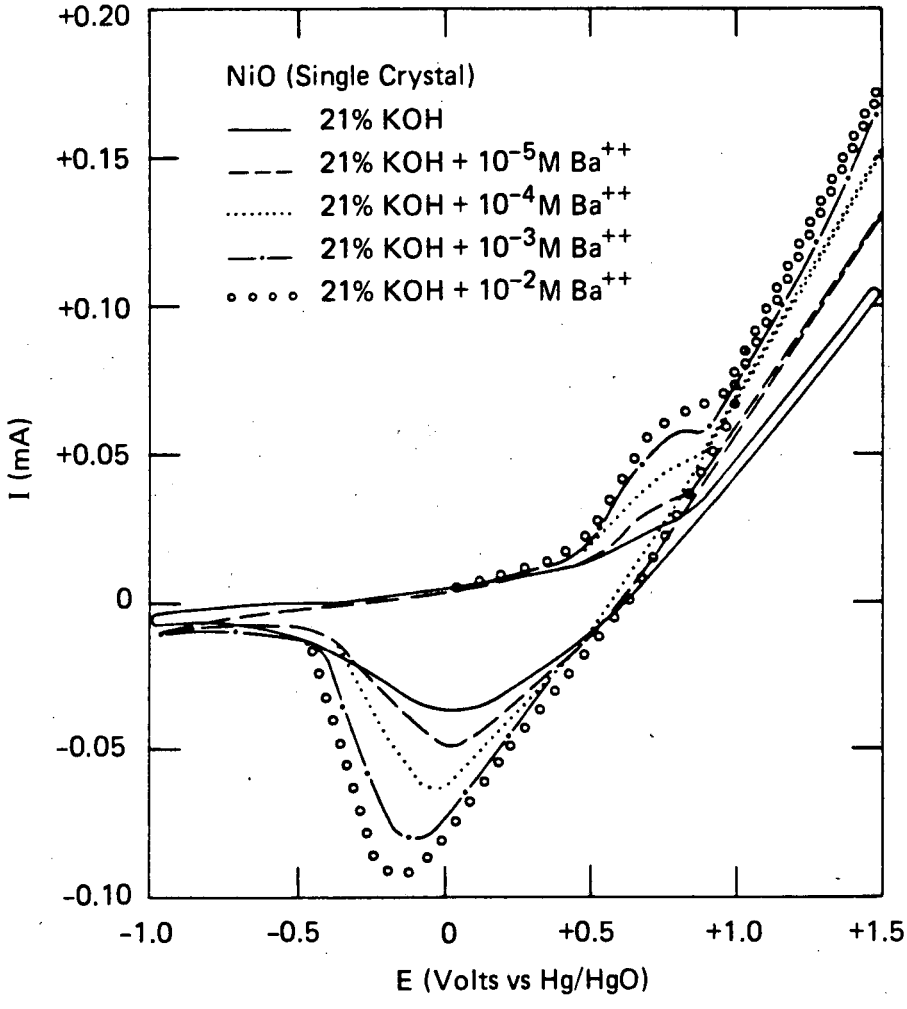

(d)

FIGURE 28 EFFECT OF BARIUM ADDITIVE ON CYCLIC VOLTAMMOGRAMS, 50 mV s^{-1} (Concluded)

REFERENCES

1. MacArthur, D.M., 1970: J. Electrochem. Soc., Vol. 117, p. 729.

2. Glarum, S.H., and J.H. Marshall, 1978: J. Electrochem. Soc., Vol. 129, p. 535.

3. Zimmerman, A.H., M.R. Martinelli, M.C. Jarnecki, and C.C. Badcock, 1981: J. Electrochem. Soc., Vol. 129, p. 289.

4. Hopper, M.A., and J.L. Ord, 1973: J. Electrochem. Soc., Vol. 120, p. 183.

5. Schrebler, R.S., J. Guzman, J.R. Vilche, and A.J. Arvia, 1978: J. Electrochem. Soc., Vol. 125, p. 1578.

6. Macagno, V.A., J.R. Vilche, and A.J. Arvia, 1980: J. Electrochem. Soc., Vol. 127, p. 301.

7. Schrebler, R.S., J. Guzman, J.R. Vilche, and A.J. Arvia, 1979: J. Appl. Electrochem., Vol. 9, p. 183.

8. Tichenor, R.L., 1952: Ind. Eng. Chem., Vol. 44, p. 973.

9. Tuomi, D., 1965: J. Electrochem. Soc., Vol. 112, p. 1.

10. Weiniger, J.L., 1982: Proceedings of the Symposium on the Nickel Electrode, J. Electrochem. Soc., Vol. 82-4, p. 1.

11. Chernykh, Yu. N., and A.A. Yakovleva, 1970: Sov. Electrochem., Vol. 6, p. 1595.

12. Angelini, E., M. Maja, and P. Spinelli, 1977: J. Phys., Vol. C-5, p. 261.

13. Briggs, G.W.D., E. Jones, and W.F.K. Wynne-Jones, 1955: Trans. Faraday Soc., Vol. 51, p. 1433.

14. Arvia, A.J., and D. Posadas, 1973: in Encyclopedia of Electrochemistry of the Elements, Vol. III, A.J. Bard, ed. (Marcel Dekker, New York).

15. Sluyters-Rehback, M., and J.H. Sluyters, 1970: in Electroanalytical Chemistry, Vol. 4, A.J. Bard, ed., pp. 1-128 (Marcel Dekker, New York).

16. Macdonald, D.D., and M.C.H. McKubre, 1982: in Modern Aspects of Electrochemistry, Vol. 14, J. O'M. Bockris, B.E. Conway, and R.E. White, eds., pp. 61-150 (Plenum, New York).

17. McKubre, M.C.H., and D.D. Macdonald, in A Treatise of Electrochemistry, Vol. 5, E. Yeager, J. O'M. Bockris, and R.E. White, eds. (to be published).

18. Madou, M.J., K., Kenoshita, and M.C.H. McKubre, submitted to Electrochim. Acta.

19. McKubre, M.C.H., 1981: "Temperature Limitation of Primary and Secondary Alkaline Battery Electrodes, Part III: The Mechanisms of Dissolution and Passivation of Iron and Zinc in Concentrated Potassium Hydroxide Solutions," Report, prepared for the Department of Energy by SRI International, Menlo Park, California under Contract 450561.

20. McKubre, M.C.H., and D.D. Macdonald, 1980: J. Electrochem. Soc., Vol. 127, p. 632.

21. MacArthur, D.M., personal communication.

22. MacArthur, D.S., 1970: J. Electrochem. Soc., Vol. 117, p. 422.

23. McKubre, M.C.H., and D.D. Macdonald, 1970: "Temperature Limitations of Alkaline Battery Electrodes, Part I," Final Report, prepared by SRI International under contract EM-78-C-01-5159, p. 99.

24. Macagno, V.A., J.R. Vilche, and A.J. Arvia, 1982: J. Electrochem. Soc., Vol. 129, p. 301.

25. Yohe, D., A. Riga, R. Greef, and E. Yeager, 1968: Electrochim. Acta, Vol. 13, p. 1351.

26. Tench, D.S., and E. Yeager, 1973: J. Electrochem. Soc., Vol. 120, p. 164.

27. McNatt, J.L., 1969: Phys. Rev. Lett., Vol., 23, p. 915.

28. Rouse, T.O., and J.L. Weiniger, 1966: J. Electrochem. Soc., Vol. 113, p. 184.

29. Drossbach, P., and J. Schultz, 1964: Electrochim. Acta, Vol. 9, p. 1391.

30. Gerischer, H., 1977: in Semiconductor Liquid-Junction Solar Cells, A. Heller, ed., p. 1, PV 77-3, The Electrochemical Society, Soft-bound Proceedings Series, Princeton, New Jersey.

31. Pourbaix, M., 1966: Atlas of Electrochemical Equilibria in Aqueous Solutions, (Pergamon-Cebelcor, Brussels).

32. Edison, T.A., 1907: U.S. Pat. 870,445C.

33. Foerster, F., 1923: Electrochemie. Wässeriger Lösungen, 4. Auflage, Verlag von Johann Ambrosius Barth, Leipzig, p. 267.

34. Hofer, K., Batterien, 1944: Vol. 12, p. 247.

35. Harivel, J.P., B. Morignat, J. Labat, and J.F. Laurount, 1966: Power Sources, Vol. 1, p. 239.

36. Cripis, D., 1981: Electrochem. Soc. Meeting, Denver (October).

37. Maladin O.G., A.V. Vasev, P.N. Bityutskü, I.S. Shoumina, and G.V. Suchkovu, 1978: Elektrokhim, Vol. 14, p. 91.

38. Weiniger, J.L., 1970: Department of the Air Force, Project 3145, General Electric Report, S-70-1025.

This report was done with support from the Department of Energy. Any conclusions or opinions expressed in this report represent solely those of the author(s) and not necessarily those of The Regents of the University of California, the Lawrence Berkeley Laboratory or the Department of Energy.

Reference to a company or product name does not imply approval or recommendation of the product by the University of California or the U.S. Department of Energy to the exclusion of others that may be suitable.

TECHNICAL INFORMATION DEPARTMENT
LAWRENCE BERKELEY LABORATORY
UNIVERSITY OF CALIFORNIA
BERKELEY, CALIFORNIA 94720